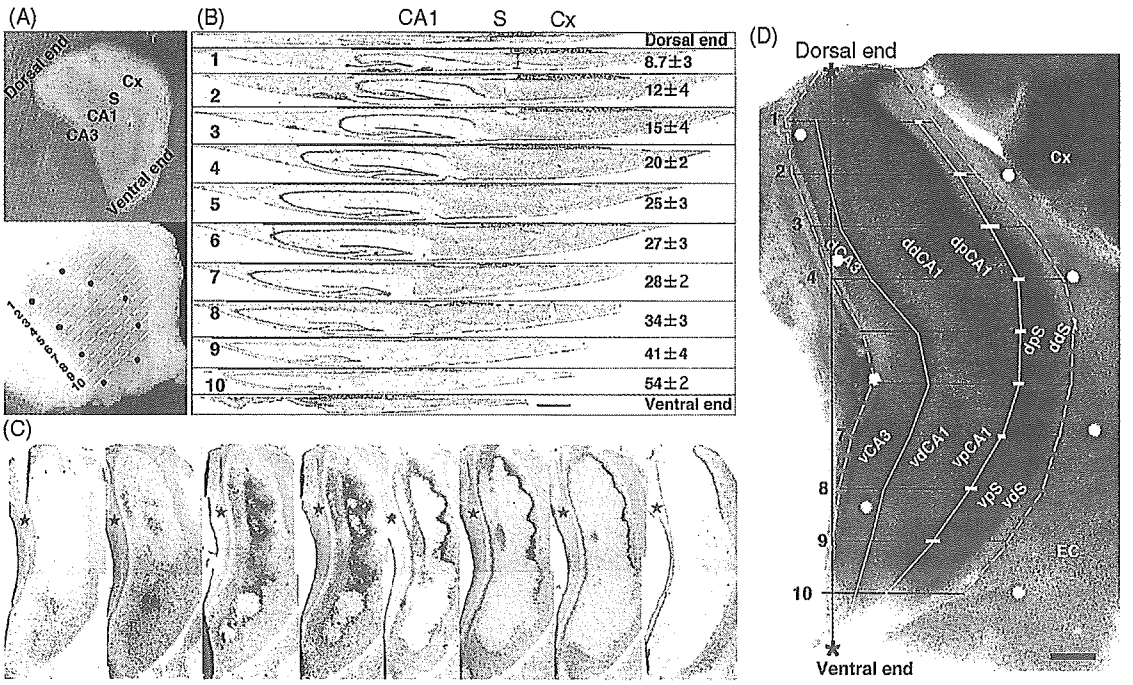

Fig. 3. Tangential sections. (A) Upper panel, dissected hippocampus containing part of the cortex. Lower panel, tangential block in which the pyramidal cell layer of the CA1 and subiculum is flattened. The black dots indicate the location of marker holes punched with a needle. Broken lines with numbers show the position of coronal sections in (B). Frozen OTC compound (white material) surrounds the tangential block. (B) Nissl-stained coronal sections (20 μm thick) from the tangential block, corresponding to the broken lines in (A). Ratio (%) of the subiculum (red line) to the CA1 (green line) + subiculum is indicated for each section (mean ± S.D., 9, tangential blocks). Note the flatness of the pyramidal cell layer. Scale bar = 1 mm. (C) Examples of the Nissl-stained tangential sections. Asterisks indicate the area used for background subtraction. (D) Two-dimensional display of the reconstructed hippocampus. A reconstructed image of the *Arc* signals obtained from C/7d/C group is shown. This image was constructed without binarization. The area including the subiculum, CA1, and CA3 is surrounded by a white broken line. The line linking the dorsal and ventral ends of the pyramidal cell layer (indicated by asterisks) was set as the longitudinal axis of the hippocampus. The border between the CA1 and subiculum was determined using the ratio of subiculum to CA1 + subiculum (see panel C), and is shown by a white line with error bars (±S.D., white horizontal bars). The border between the CA1 and CA3 is also shown by a thin white line. Black horizontal lines with numbers correspond to the position of coronal sections that are shown in panel B. White holes indicate marker holes generated by a needle. S, subiculum; dpS, dorsal–proximal subiculum; ddS, dorsal–distal subiculum; vpS, ventral–proximal subiculum; vdS, ventral–distal subiculum; dpCA1, dorsal–proximal CA1; ddCA1, dorsal–distal CA1; vpCA1, ventral–proximal CA1; vdCA1, ventral–distal CA1; dCA3, dorsal CA3; vCA3, ventral CA3; Cx, cortex; EC, entorhinal cortex. Scale bar = 1 mm.

Arc mRNA level was observed in the CA1 and subiculum of animals in the C/1d/C group (Fig. 2C and E). There seemed to be no obvious differences in the mRNA expression pattern between these two groups. *Arc* signals were not detected in the pyramidal cell layer of the naive group. In contrast, both of the N/C and C/1d/C groups showed little increase in the *Arc* signals in CA3 and dentate gyrus (Fig. 2D and F). Thus, the analysis with the coronal sections revealed that the exposure to context and shock induces *Arc* mRNA expression in the CA1 and subiculum. This analysis, however, did not examine the *Arc* expression profile in the entire hippocampus.

3.3. Preparation of sections tangential to the pyramidal cell layer

Pyramidal cells in the CA1 region and the subiculum are located at the surface of the spherical hippocampus as a thin multi-cellular layer. This topographic organization implies that the entire population of the pyramidal cells could be displayed in a two-dimensional plane. The spherical surface corresponding to the pyramidal cell layer of the dissected hippocampus was pushed against a flat plate, flattened, and frozen immediately (tangential block, Fig. 3A). When the tangential block was sliced at right angles to the flat plane (dotted lines in Fig. 3A bottom), we observed that the pyramidal cell layer of the CA1 and subiculum regions are linearly arrayed in all the sections (Fig. 3B), indicating that the pyramidal cell layer approximates a flattened plane. The frozen tangential block was then sliced in parallel with the flat plane to generate 20–30 serial sections (tangential sections) that include the entire population of the pyramidal cells in the subiculum, CA1, and CA2 regions and a part of pyramidal cells in the CA3 region.

3.4. Reconstruction of a two-dimensional map of the pyramidal cell layer

Each tangential section was hybridized with a DIG-labeled *Arc* cRNA probe and *Arc* signals were detected with the alkaline phosphatase–NBT system, followed by de-staining of the DIG signals and re-staining with Nissl.

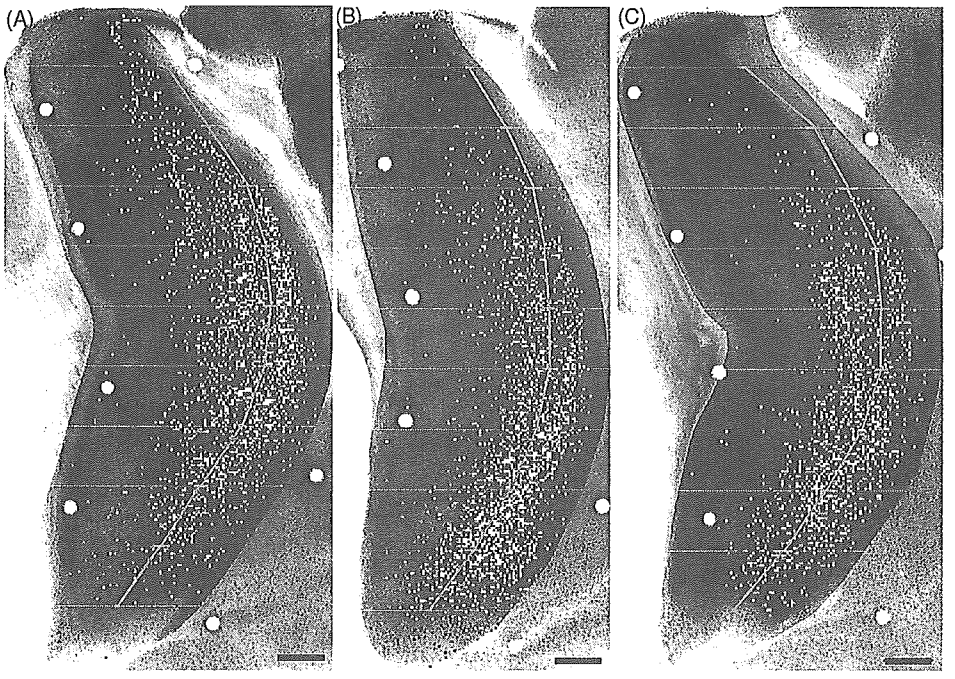

Fig. 4. *Arc* signal distribution on the two-dimensional map. Typical representations of the *Arc* signals on the hippocampus from N/C (A), C/1d/C (B), and C/7d/C (C) rats. The *Arc* signal was binarized so that the positive pixels occupied 0.5% of the total pixels in the area surrounded by broken line in Fig. 3D (see Section 2 for details). The total number of pixels within the area corresponding to the subiculum and CA1 is approximately 1.5×10^7. The red line with error bars (±S.D., horizontal bars) indicates the presumptive border between subiculum and CA1 based on the calculation in Fig. 3B. (A–C) Pseudo-coloring, purple, cyan or yellow, was assigned to each area of 20 × 20 pixels when it contained 1–3, 4–7 or >8 *Arc*-positive pixels, respectively. Scale bar = 1 mm.

Images of *Arc* and Nissl signals were obtained with a cooled CCD camera. Examples of each tangential section stained with Nissl are shown in Fig. 3C. Images of each tangential section were then stacked, using Image Pro Express software to build a two-dimensional image of the entire population of pyramidal cells. Fig. 3D shows a reconstructed map of the tangential sections hybridized with the *Arc* probe. The overall organization of the reconstructed map resembles the hippocampal flat map that has been modeled from an equally spaced series of Nissl-stained frontal sections (Swanson et al., 1978; Petrovich et al., 2001). Thus, with the technique developed here, we could easily represent the entire population of pyramidal cells in the CA1 and subiculum on a two-dimensional plane.

3.5. Distribution of the Arc mRNA signals on the two-dimensional map

Distribution of the *Arc* signal was displayed on the two-dimensional map (Fig. 4). Reconstructed images of the N/C group showed uniformly distributed *Arc* signals throughout the pyramidal cell layer with relatively dense signals along the border of the CA1 and the subiculum (Fig. 4A, see Fig. 3D for topographic assignment). In contrast, a net shift of the *Arc* signals toward the ventral area was observed in pre-exposed groups, again with higher signals at the border between the CA1 and subiculum (C/1d/C and C/7d/C) (Fig. 4B and C). Two-dimensional maps constructed from the other test animals (three animals per group) showed essentially the same *Arc* distribution patterns (data not shown).

3.6. Net shift of neural activity from the dorsal to ventral side of the pyramidal cell layer after fear conditioning

We quantified the distribution of the *Arc* signals in the pyramidal cell layer. The histogram in Fig. 5A shows the relative signal distribution along the longitudinal axis from dorsal to ventral hippocampus of individual animals. In the N/C group, the *Arc* signal distributed symmetrically along the longitudinal (dorsal–ventral) axis with a peak around the central area. The histograms for the pre-trained groups (C/1d/C and C/7d/C) did not show a symmetrical distribution pattern. An additional peak is evident at the ventral side of the hippocampus in the C/1d/C group. An overall shift of the signal toward the ventral side is also evident for the CS/7d/CS group. Cumulative analysis clearly demonstrates the net shift of *Arc* signals toward the ventral side in the pre-exposed groups (Fig. 5B) (two-way ANOVA, $F_{(2,897)} = 4.38$, $p = 0.013$; Fisher's PLSD, N/C versus C/1d/C, $p < 0.01$, N/C versus C/7d/C, $p = 0.069$). *Arc* signals were not detected in the pyramidal cell layer of the C/1d/N group (not shown), indicating that the *Arc* signals observed in the pre-exposed group were induced by the context and shock 30 min prior to the *Arc* analysis rather than the experience of the previous day.

Taken together, the previous experience of exposure to context and shock influenced the neural activation

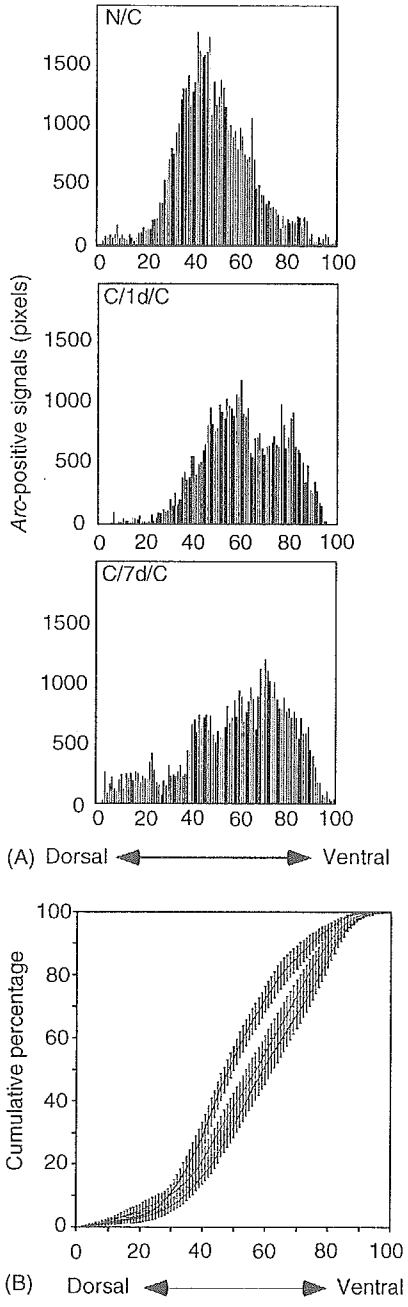

Fig. 5. Net shift of the *Arc*-positive signals from dorsal to ventral hippocampus after fear conditioning. The *Arc* signal was binarized so that the positive pixels occupied 0.5% of the total pixels in the subiculum and CA1. The area containing the subiculum and CA1 on the two-dimensional map was divided into 100 equally spaced areas along the longitudinal axis (shown in Fig. 3D) from the dorsal to ventral end. The number of *Arc*-positive pixels was counted for each area. (A) Histograms showing the distribution of the number of *Arc*-positive pixels along the longitudinal axis. (B) Cumulative percentage of the *Arc*-positive pixels. Data in panel A are displayed as a cumulative curve. Data from three animals per group were averaged (mean ± S.E.M.). Black, N/C; red, C/1d/C; green, C/7d/C.

pattern following the second exposure to context and shock. These shifts may represent a reorganization of the hippocampal neural circuit associated with the fear-conditioned memory trace.

4. Discussion

4.1. Construction of a two-dimensional map

In the present study, we developed a novel mapping method that allowed us to detect the neural activity of the entire population of pyramidal cells in the CA1/subiculum on a two-dimensional plane. All the pyramidal cells in the CA1 and subiculum were included in a total of 20–30 serial tangential sections, which easily allowed us to construct a two-dimensional flat map of the CA1 and subiculum regions. Configuration of the flat map thus constructed is quit similar to that made from a large number of coronal Nissl-stained sections (Swanson et al., 1978; Petrovich et al., 2001). Combined with the *Arc* mRNA hybridisation, the two-dimensional map technique is able to display the neural activity of the entire CA1 and subiculum regions at a spatially high resolution, even at the single cell level. Thus, the tangential section/two-dimensional map technique is a powerful method, in combination with electrophysiological recording of individual neurons in rodents and functional imaging such as functional MRI and PET in human, for the analysis of the overall pattern of neural activity in the CA1 and subiculum that is involved in information processing during memory acquisition, consolidation, retrieval, and reconsolidation.

4.2. Role of the ventral hippocampus revealed by analysis of the two-dimensional map

The most pronounced feature of the *Arc* signal distribution in the two-dimensional map is the net shift of *Arc*-positive cells from dorsal to ventral CA1/subiculum in the pre-exposed group (C/1d/C and C/7d/C). Both groups of rats, non-pre-exposed and pre-exposed, received the same input 30 min prior to sacrifice on the last day. Thus, the shift can be attributed to the experience of pre-exposure to context and shock, 1 or 7 days prior to shock on the reconditioning day. In the N/C group, the animals were exposed to the conditioned box as a novel environment 30 min prior to the *Arc* analysis. These animals showed a searching behavior and acquired the surrounding spatial information until they received electric foot-shocks. In contrast, animals of the pre-exposed groups showed a freezing behavior at the beginning of the reconditioning session, as they had already learned the association between context and shock. The difference in the distribution of the *Arc*-positive cells, therefore, reflects the different performance of these two groups of animals, and may be caused by the difference in the information processing between encoding/consolidation in the N/C group and retrieval/re-encoding/reconsolidation in the pre-exposed group.

Contextual fear conditioning requires the hippocampus, specifically the ventral hippocampus, and the amygdala (Kim and Fanselow, 1992; Kim and Davis, 1993; Maren et al., 1997; Fanselow, 2000; Pare et al., 2004). The amygdala is

implicated in emotion, memory and social behavior, and plays a critical role in fear memory retrieval (LeDoux, 2000; Rodrigues et al., 2004). Afferent and efferent fibers from the amygdala project mainly to the ventral hippocampus, in particular, to the ventral–proximal CA1 and ventral–proximal subiculum (Naber and Witter, 1998; Petrovich et al., 2001), precisely where the most intense *Arc* signals were detected in the pre-exposed group. The ventral–proximal subiculum is the major origin of output from the hippocampus to the amygdala and anterior hypothalamic nucleus, which both play a central role in the expression of aggressive–defensive behavior (Naber and Witter, 1998; Kishi et al., 2000). Therefore, the relative increase in neural activity in the ventral–proximal CA1/subiculum may reflect the reinforcement of the amygdala and ventral–proximal CA1/subiculum circuit by repeated fear experiences, which induce the fear memory retrieval process. Consistent with this model, imaging studies in human subjects reveal that the encoding and retrieval of memories appears to involve the anterior (corresponding to dorsal in rodents) and posterior (ventral in rodents) hippocampus, respectively (Lepage et al., 1998; Zeineh et al., 2003). The relative increase in neural activity in the ventral–proximal CA1/subiculum probably reflects the contribution of this area to the retrieval of fear memory. This does not, however, necessarily exclude the possibility that reconditioning itself may affect the *Arc* expression profile.

Previously consolidated fear memories enter a labile and unstable state when recalled. Memories then enter a new phase referred to as the reconsolidation process, in order to be reinforced and maintained (Misanin et al., 1968; Mactutus et al., 1979; Nader et al., 2000). In this context, the net shift of the *Arc* signals from dorsal to ventral hippocampus in the pre-exposed groups may also reflect an involvement of the ventral hippocampus in reconsolidation after retrieval. Thus, our results suggest that the reconsolidation of fear memory uses specific neural pathways that are distinct from those utilized during the consolidation of a new memory.

Acknowledgments

We thank members of Inokuchi lab for their helpful discussions. This work was supported by Special Coordinate Funds for Promoting Science and Technology, and grants for Scientific Research on Priority Areas (A)-Neural Circuit Project and (C)-Advanced Brain Science Project, from the Ministry of Education, Culture, Sports, Science and Technology of the Japanese Government to K.I.

References

Amaral, D.G., Witter, M.P., 1995. Hippocampal formation. In: Paxinos, G. (Ed.), The Rat Nervous System. Academic Press, San Diego, pp. 443–493.

Bannerman, D.M., Grubb, M., Deacon, R.M., Yee, B.K., Feldon, J., Rawlins, J.N., 2003. Ventral hippocampal lesions affect anxiety but not spatial learning. Behav. Brain Res. 139, 197–213.

Brown, M.W., Aggleton, J.P., 2001. Recognition memory: what are the roles of the perirhinal cortex and hippocampus? Nat. Rev. Neurosci. 2, 51–61.

Eichenbaum, H., 2004. Hippocampus: cognitive processes and neural representations that underlie declarative memory. Neuron 44, 109–120.

Fanselow, M.S., 2000. Contextual fear, gestalt memories, and the hippocampus. Behav. Brain Res. 110, 73–81.

Guzowski, J.F., Lyford, G.L., Stevenson, G.D., Houston, F.P., McGaugh, J.L., Worley, P.F., Barnes, C.A., 2000. Inhibition of activity-dependent arc protein expression in the rat hippocampus impairs the maintenance of long-term potentiation and the consolidation of long-term memory. J. Neurosci. 20, 3993–4001.

Guzowski, J.F., McNaughton, B.L., Barnes, C.A., Worley, P.F., 1999. Environment-specific expression of the immediate–early gene *Arc* in hippocampal neuronal ensembles. Nat. Neurosci. 2, 1120–1124.

Guzowski, J.F., Setlow, B., Wagner, E.K., McGaugh, J.L., 2001. Experience-dependent gene expression in the rat hippocampus after spatial learning: a comparison of the immediate–early genes *Arc*, c-*fos*, and *zif268*. J. Neurosci. 21, 5089–5098.

Hampson, R.E., Simeral, J.D., Deadwyler, S.A., 1999. Distribution of spatial and nonspatial information in dorsal hippocampus. Nature 402, 610–614.

Kelly, M.P., Deadwyler, S.A., 2003. Experience-dependent regulation of the immediate–early gene *Arc* differs across brain regions. J. Neurosci. 23, 6443–6451.

Kim, J.J., Fanselow, M.S., 1992. Modality-specific retrograde amnesia of fear. Science 256, 675–677.

Kim, M., Davis, M., 1993. Lack of a temporal gradient of retrograde amnesia in rats with amygdala lesions assessed with the fear-potentiated startle paradigm. Behav. Neurosci. 107, 1088–1092.

Kishi, T., Tsumori, T., Ono, K., Yokota, S., Ishino, H., Yasui, Y., 2000. Topographical organization of projections from the subiculum to the hypothalamus in the rat. J. Comp. Neurol. 419, 205–222.

Kjelstrup, K.G., Tuvnes, F.A., Steffenach, H.A., Murison, R., Moser, E.I., Moser, M.B., 2002. Reduced fear expression after lesions of the ventral hippocampus. Proc. Natl. Acad. Sci. U.S.A. 99, 10825–10830.

LeDoux, J.E., 2000. Emotion circuits in the brain. Annu. Rev. Neurosci. 23, 155–184.

Lepage, M., Habib, R., Tulving, E., 1998. Hippocampal PET activations of memory encoding and retrieval: the HIPER model. Hippocampus 8, 313–322.

Lisman, J.E., 1999. Relating hippocampal circuitry to function: recall of memory sequences by reciprocal dentate–CA3 interactions. Neuron 22, 233–242.

Mactutus, C.F., Riccio, D.C., Ferek, J.M., 1979. Retrograde amnesia for old (reactivated) memory: some anomalous characteristics. Science 204, 1319–1320.

Maren, S., Aharonov, G., Fanselow, M.S., 1997. Neurotoxic lesions of the dorsal hippocampus and Pavlovian fear conditioning in rats. Behav. Brain Res. 88, 261–274.

Misanin, J.R., Miller, R.R., Lewis, D.J., 1968. Retrograde amnesia produced by electroconvulsive shock after reactivation of a consolidated memory trace. Science 160, 554–555.

Morris, R.G.M., Garrud, P., Rawlins, J.N.P., O'Keefe, J., 1982. Place navigation impaired in rats with hippocampal lesions. Nature 297, 681–683.

Moser, M.B., Moser, E.I., 1998. Functional differentiation in the hippocampus. Hippocampus 8, 608–619.

Naber, P.A., Witter, M.P., 1998. Subicular efferents are organized mostly as parallel projections: a double-labeling, retrograde-tracing study in the rat. J. Comp. Neurol. 393, 284–297.

Nader, K., Schafe, G.E., Le Doux, J.E., 2000. Fear memories require protein synthesis in the amygdala for reconsolidation after retrieval. Nature 406, 722–726.

O'Keefe, J., Dostrovsky, J., 1971. The hippocampus as a spatial map. Preliminary evidence from unit activity in the freely-moving rat. Brain Res. 34, 171–175.

Pare, D., Quirk, G.J., Ledoux, J.E., 2004. New vistas on amygdala networks in conditioned fear. J. Neurophysiol. 92, 1–9.

Petrovich, G.D., Canteras, N.S., Swanson, L.W., 2001. Combinatorial amygdalar inputs to hippocampal domains and hypothalamic behavior systems. Brain Res. Brain Res. Rev. 38, 247–289.

Pittenger, C., Huang, Y.Y., Paletzki, R.F., Bourtchouladze, R., Scanlin, H., Vronskaya, S., Kandel, E.R., 2002. Reversible inhibition of CREB/ATF transcription factors in region CA1 of the dorsal hippocampus disrupts hippocampus-dependent spatial memory. Neuron 34, 447–462.

Richmond, M.A., Yee, B.K., Pouzet, B., Veenman, L., Rawlins, J.N., Feldon, J., Bannerman, D.M., 1999. Dissociating context and space within the hippocampus: effects of complete, dorsal, and ventral excitotoxic hippocampal lesions on conditioned freezing and spatial learning. Behav. Neurosci. 113, 1189–1203.

Rodrigues, S.M., Schafe, G.E., LeDoux, J.E., 2004. Molecular mechanisms underlying emotional learning and memory in the lateral amygdala. Neuron 44, 75–91.

Swanson, L.W., Wyss, J.M., Cowan, W.M., 1978. An autoradiographic study of the organization of intrahippocampal association pathways in the rat. J. Comp. Neurol. 181, 681–715.

Zeineh, M.M., Engel, S.A., Thompson, P.M., Bookheimer, S.Y., 2003. Dynamics of the hippocampus during encoding and retrieval of face-name pairs. Science 299, 577–580.

European Journal of Neuroscience, Vol. 22, pp. 1338–1348, 2005

Homer 1a enhances spike-induced calcium influx via L-type calcium channels in neocortex pyramidal cells

Kenji Yamamoto,[1,2] Yu Sakagami,[1,3] Shigeki Sugiura,[4] Kaoru Inokuchi,[5] Shun Shimohama[2] and Nobuo Kato[1]
[1]Department of Integrative Brain Science, Kyoto University Graduate School of Medicine, Kyoto 606–8501, Japan
[2]Department of Neurology, Kyoto University Graduate School of Medicine, Kyoto, Japan
[3]Department of Psychiatry, Kyoto University Graduate School of Medicine, Kyoto, Japan
[4]Nara Medial University, Kashihara, Japan
[5]Mitsubishi Kagaku Institute of Life Sciences (MITILS), Machida, Japan

Keywords: calcium channels, calcium influx, electroconvulsive shock, glutamate receptor, rat, scaffold protein

Abstract

The scaffold protein family Homer/Vesl serves to couple surface receptors or channels with endoplasmic calcium release channels. Homer 1a/Vesl-1S is regarded as regulating such coupling in an activity-dependent manner. The present calcium photometry and electrophysiological measurement revealed that Homer 1a up-regulates voltage-dependent calcium channels (VDCCs), depending on inositol-1,4,5-trisphosphate (IP_3) receptors (IP_3Rs). In rat neocortex pyramidal cells, intracellular injection by diffusion from the patch pipette (referred to as 'infusion') of Homer 1a protein enhanced spike-induced calcium increase, depending on both the protein concentration and spike frequency. Induction of this enhancement was disrupted by blockers of key molecules of the mGluR–IP_3 signalling pathway, including metabotropic glutamate receptors (mGluRs), phospholipase C and IP_3Rs. However, infusion of IP_3 failed to mimic the effect of Homer 1a, suggesting requirement for a second Homer 1a-mediated signalling as well as the mGluR–IP_3 signalling. In contrast to the induction, maintenance of this enhancement was independent of the mGluR–IP_3 signalling, taking the form of augmented calcium influx via L-type VDCCs. Presumably due to the VDCC up-regulation, threshold currents for calcium spikes were reduced. Given that Homer 1a induction is thought to down-regulate neural excitability and hence somatic spike firing, this facilitation of calcium spikes concomitant with such attenuated firing may well have a critical impact on bi-directional synaptic plasticity.

Introduction

Homer 1a/Vesl-1S is one of the Homer proteins that constitute the scaffold protein family Homer. Molecules known to link Homers include metabotropic glutamate receptors (mGluRs), inositol-1,4,5-trisphosphate receptors (IP_3Rs), ryanodine receptors, transient receptor potential channels, and Shanks (Tu *et al.*, 1998; Kennedy, 2000; Sheng & Kim, 2000; Ehlers, 2002; Feng *et al.*, 2002; Westhoff *et al.*, 2003; Yuan *et al.*, 2003). As an immediate-early gene product, Homer 1a is inducible by convulsion or tetanization leading to long-term potentiation (LTP; Brakeman *et al.*, 1997; Kato *et al.*, 1997). It has been suggested that this activity-dependently inducible protein in turn regulates neural activity. Homer 1a overexpression increases the threshold for amygdala kindling (Potschka *et al.*, 2002; Schwarz *et al.*, 2003), and reduces the magnitude of LTP in the sliced hippocampus, presumably by weakening postsynaptic responses during tetanization (Schwarz *et al.*, 2003). In *Homer 1*-knockout mice, on the other hand, enhancement of LTP has been demonstrated (Schwarz *et al.*, 2003). These findings raise the possibility that Homer 1a may mediate a feedback loop, initiated by intense neural activity, which would ultimately down-regulate neural excitability.

Recently we have described a feedback regulation of spike firing dependent on IP_3Rs and mGluRs, both of which are Homer-attachable molecules (Yamada *et al.*, 2004). This feedback is based on an action potential-induced supra-linear increase in $[Ca^{2+}]_i$ in visual cortex pyramidal cells. The supra-linearity arises because action potential-induced Ca^{2+} influx triggers Ca^{2+} release from inositol-1,4,5-trisphosphate (IP_3) receptors sensitized by a prior increase in IP_3 [IP_3-assisted calcium-induced calcium release (CICR); Yamamoto *et al.*, 2000; Nakamura *et al.*, 1999; Power & Sah, 2002]. IP_3-assisted CICR aimed at small-conductance calcium-activated K (SK) channels, thereby down-regulating the spike firing that initially caused IP_3-assisted CICR (Yamamoto *et al.*, 2002a,b; Yamada *et al.*, 2004). Thus, this supra-linear increase in $[Ca^{2+}]_i$ is enabled in a manner dependent on IP_3. Although we initially made use of muscarinic acetylcholine receptor activation (Yamamoto *et al.*, 2000), activation of group I mGluRs also suffices to provide the requisite IP_3 (Yamada *et al.*, 2004). Given that Homers can be attached to both IP_3Rs and mGluRs, the machinery for this supra-linear Ca^{2+} increase (IP_3-assisted CICR) may well involve Homers. The present study therefore investigated whether Homer 1a affects IP_3-assisted CICR. First, intracellular injection by diffusion from the patch pipette (referred to as 'infusion') of Homer 1a protein was shown to amplify Ca^{2+} increases induced by single action potentials, and then we set out to characterise this Homer-induced Ca^{2+} increase. To our surprise, it turned out that the amplified Ca^{2+} increase is attributable to enhancement of Ca^{2+} influx rather than Ca^{2+} release. We thus studied the underlying mechanism and functional significance of this novel Homer-induced enhancement of Ca^{2+} influx.

Correspondence: Dr Nobuo Kato, as above.
E-mail: f50207@sakura.kudpc.kyoto-u.ac.jp

Received 17 January 2005, revised 25 May 2005, accepted 10 June 2005

doi:10.1111/j.1460-9568.2005.04278.x

Materials and methods

All experiments were performed in accordance with the guiding principle of the Physiological Society of Japan and with the approval of the Animal Care Committee of Kyoto University Graduate School of Medicine.

Slice preparation

Wistar rats (16–18 days old) were killed by prompt decapitation under ether anaesthesia. The brain was dissected out and immersed in bathing medium (pH 7.4; 2–5 °C) containing (in mM): NaCl, 124; KCl, 3.3; KH_2PO_4, 1.3; $NaHCO_3$, 26; $CaCl_2$, 2.5; $MgSO_4$, 2.0; and glucose, 20. Slices of the visual cortex were cut with a slicer at 200 μm (Dosaka, Kyoto, Japan).

Electroconvulsive shock (ECS)

We used an electrical stimulator designed for electroconvulsion therapy in humans (C-2 type; Sakai Ltd, Tokyo, Japan). Both auricles of each rat were humidified with bathing medium and alligator clamps were attached. In some occasions, when rats tried to remove the clamps, we lightly anaesthetized the animal with ether or simply waited for them to calm down, so as to minimize uneasiness. Two volleys of alternating current (6 pHz, 90 V) were applied interaurally at an interval of 5 min. On passing the current, the whole body of the animal became rigid. At 10–20 s after the first volley, tonic–clonic seizure started and lasted for 20–40 s. After the second volley, a milder seizure lasting for a shorter time was observed. Within 1 h, animals looked as normal as before the volleys. Animals were killed 10–20 min or 6 h later. Slices were then cut in the same way as described for normal rats.

Electrophysiology

Slices were placed in a recording chamber on the stage of an upright microscope (BHWI; Olympus) with a ×40 water-immersion objective (WPlanFl 40×UV). The chamber was continuously perfused with bathing medium (25 °C) bubbled with a mixture of 95% O_2 and 5% CO_2. For recording, we used patch pipettes (resistance 4–10 MΩ) filled with a solution (pH 7.3) containing (in mM) KCl, 7; K-gluconate, 144; KOH, 10; and HEPES, 10. Whole-cell recordings were made from layer II-III pyramidal cells that had sufficiently negative resting membrane potentials (more negative than −55 mV) without spontaneous action potentials. Membrane potentials were recorded in the current-clamp mode (Axoclamp 1D; Axon Instruments, California, USA) and digitized at 10 kHz (Digidata 1200 and pCLAMP7, Axon Instruments).

For recording Ca^{2+} currents under voltage clamp, tetrodotoxin (TTX; 1 μM; Sigma) and tetraethylammonium chloride (TEA; 20 mM; Nacalai, Kyoto, Japan) were added to the bathing medium; when TEA was used, the concentration of NaCl was reduced to 104 mM. Patch pipettes were filled with a Cs-based solution (to block K^+ channels pH 7.3) containing (in mM) Cs-gluconate, 133; CsCl, 6; TEA, 9; HEPES, 9; and QX-314, 5. Ca^{2+} currents induced by step depolarizations from −70 mV (holding potential) to −50, −30, −10 and +10 mV for 200 ms were recorded in the voltage-clamp mode. When barium-containing bathing medium was used, $MgSO_4$ was replaced with $MgCl_2$.

Elicitation of calcium spikes

To elicit Ca^{2+} spikes in the current-clamp mode, depolarizing currents (20–240 pA for 50 ms) were injected through the patch pipette according to the methods described by Young & Yang (2004). Currents of varying intensities were injected at 10-s intervals. Under sodium and potassium channel blockade by TTX (1 μM) and TEA (20 mM), this current injection elicited action potentials, in an all-or-none fashion, which are attributable to Ca^{2+} currents (Ca^{2+} spikes). We determined the threshold current for the elicitation of these Ca^{2+} spikes in various experimental conditions.

Calcium photometry

Fluorimetry was performed as described (Yamamoto *et al.*, 2002a, b). Briefly, fura-2 (0.2 mM; Dojindo Ltd, Japan) was loaded for at least 5 min after whole-cell break-in. Four brief depolarizing currents were injected to evoke a train of action potentials (+0.2 to +0.6 nA, 5–10 ms) and, simultaneously, Ca^{2+} signals were measured (for 5 s in total for each trial). Ca^{2+} signals were measured from the soma with a photomultiplier (OSP-10, Olympus) attached to the microscope (BHWI, Olympus). Fluorescence signals excited at 360 nm were measured without current injections. To estimate absolute changes in the Ca^{2+} concentration, we defined $-\Delta F_{380}/F_{360}$ as the index (Isomura & Kato, 1999). In this formula, ΔF_{380} is the difference between the 380-nm-excited fluorescence intensity (F_{380}) in the resting state and the fluorescence intensity at a given time during the trial, and F_{360} is the 360 nm-excited fluorescence intensity measured shortly before the test measurement with 380-nm-excited fluorescence. All the Ca^{2+} increases were expressed in units of $-\Delta F_{380}/F_{360}$. Ca^{2+} increases induced by the four-spike trial were averaged over three trials to provide the data plots shown in the figures.

Recombinant proteins and antibodies

Homer proteins and rabbit anti-Homer 1a or 1b/c antibodies were obtained and characterized as described (Kato *et al.*, 1997, 2001). Vesl-1 L/Homer 1c was first collected as the GST-fusion form and then refined to be GST-free (MW 47 kDa). We regard Vesl-1 L/Homer 1c as representing the two long Homer 1 proteins, thus referring to it as Homer 1b/c henceforth. Antibodies (Ab) against Homer 1a and 1b/c were rabbit polyclonal antibodies (both 0.4 μg/mL).

Also, Homer 1a was obtained separately by the following method. Rat Homer 1a cDNA was isolated by polymerase chain reaction (PCR). Amplification of the coding sequence of rat Homer 1a was performed by using rat brain QUICK-clone cDNA (Clontech, Palo Alto, California, USA) as a template for PCR. Oligonucleotide primers (5′-GAT GGA TCC ATG GGG GAACAACCTATCTTCAGCAC-3′; 5′-CGT TGG TAC CAT CTC ATT TAA TCA TGA TTG CTG-3′) were designed to incorporate upstream and downstream *Bam*HI and *Kpn*I sites, respectively. The PCR reaction was performed with Advantage2 polymerase (Clontech) as follows: 30 cycles of 30 s at 94 °C, 30 s at 60 °C and 2 min at 68 °C. Upon partial digestion of the obtained PCR product with *Kpn*I, a 580-bp *Bam*HI-*Kpn*I fragment was cloned into pUC19 for nucleotide sequence determination. It has been reported that nucleotide 539 of rat Homer 1a coding sequence (GenBank accession no. AJ276327) was T. Although our results showed that this nucleotide was C, this base substitution was the third letter of histidine code and did not result in amino acid change. After verifying the sequence, a 590-bp *Bam*HI-*Eco*RI fragment was subcloned into expression vector pGEX-6P-1 (Amersham Pharmacia Biotech) for the following purification of fusion protein using glutathione Sepharose 4B. A GST–Homer 1a fusion protein was expressed in *E. coli* BL21 and affinity-purified with glutathione-Sepharose 4B (Amersham Pharmacia Biotech) according to the

manufacturer's instructions. The protein (MW 49 kDa) was dialysed against buffer A [in mM: Hepes (pH 7.3), 10; KCl, 7; potassium gluconate, 144] at 4 °C.

Drugs used

Depending on the purpose of the experiments, 2-methyl-6-(phenylethynyl)-pyridine (MPEP; 10 μM), (RS)-1-aminoindan-1,5-dicarboxylic acid (AIDA; 1 mM), U-73122 (4 μM), cyclopiazonic acid (CPA; 30 μM), low molecular weight heparin (Heparin, 4 mg/mL), nimodipine (20 μM), BayK8644 (1 μM), nickel ions (500 or 50 μM), carbachol (10 μM) (all purchased from Sigma Inc.), ω-conotoxin GVIA (1 μM; Alomone Laboratories, Jerusalem), and/or ω-agatoxin IVA (100 nM; Alomone Laboratories) were applied into the bath (bath-applied). In experiments designed to study drug-dependence of the maintenance of enhanced calcium increase, drugs were applied after recording or photometry had started. To study drug-dependence of its induction, drugs were applied >10 min prior to recording or photometry, except that U-73122 was applied immediately before recording because of its tendency to induce a slight depolarization with a long incubation time. In previous experiments (Yamamoto *et al.*, 2002a), we used both the conventional heparin (MW 12 kDa), intracellularly applied, and a membrane-permeable, low molecular weight heparin (MW 3 kDa), bath-applied, and showed that the two heparins are similarly effective. In the present experiments, we used the low molecular weight version (4 mg/mL) for practical reasons.

Homer protein (Homer 1a or Homer 1b/c), anti-Homer 1a or Homer 1b/c antibodies, or IP_3 (200 μM; Dojindo Ltd) was contained in the patch pipette internal solution and distributed into the cell by diffusion, for 5–10 min after the break-in, before the recording session was started. Because no noticeable increase in effects was observed thereafter, a period of 10 min was regarded to be sufficiently long for diffusion.

Data analysis

Data are expressed as mean ± SEM. Paired or unpaired *t*-tests were used for parametric statistics. For comparing thresholds for Ca^{2+} spikes, Mann–Whitney rank-sum tests were used, because applied currents were discrete variables. Statistical tests for Ca^{2+} currents were made by using the peak values (evoked by the voltage step from −70 to −10 mV).

Results

Intracellular infusion of Homer 1a enhanced spike-induced calcium increases

Injection of a series of four depolarizing pulses into visual cortex pyramidal cells evoked a train of four spikes (Fig. 1, A1, Inset bottom, 8Hz; top, 18 Hz), which evoked a stepwise or gradual increase in intracellular Ca^{2+} (Fig. 1A, control: grey trace for 8 Hz, black trace for 18 Hz), as previously described (Yamamoto *et al.*, 2000). In some cases, a clear four-step increase in Ca^{2+} was observed, corresponding to the four-spike train, whereas the four-step pattern was less typical in other cases as shown in Fig. 1A. The frequencies of spike trains used here were 8 and 18 Hz. The peak amplitude of the Ca^{2+} rise was 0.18 ± 0.01 ($n = 5$) in units of $-\Delta F_{380}/F_{360}$ at both frequencies.

At both frequencies, these spike-induced Ca^{2+} increases were enhanced by intracellular infusion of Homer 1a (12.9 μg/mL; Fig. 1B, top), and were significantly larger than controls (0.27 ± 0.01 at 8 Hz, $P < 0.001$, $n = 5$; 0.32 ± 0.01 at 18 Hz, $P < 0.001$). The Homer 1a-induced enhancement of Ca^{2+} rise was not only frequency-dependent but also dose-dependent. The enhancement was still significant (0.24 ± 0.01 at 8 Hz, $P < 0.01$, $n = 6$; 0.28 ± 0.01 at 18 Hz, $P < 0.001$) with the concentration of Homer 1a reduced to one third (3.88 μg/mL; Fig. 1B, middle), but was no longer significant when reduced to one-tenth (1.29 μg/mL; 0.19 ± 0.01 at 8 Hz, $n = 5$; 0.20 ± 0.01 at 18 Hz; Fig. 1B, bottom). In contrast to Homer 1a, Homer 1b/c did not significantly enhance spike-induced Ca^{2+} rises at either frequency (0.18 ± 0.01 at 8 and 18 Hz, $n = 6$; Fig. 1C). It has thus been shown that Homer 1a specifically enhances spike-induced Ca^{2+} increases (Fig. 1D).

We further studied the Homer 1a-induced enhancement of Ca^{2+} rise in terms of both the mechanism of induction and the way this enhancement is maintained. In the experiments described below, the concentration of Homer 1a was always 3.88 μg/mL, and 18-Hz spike trains were applied. Homer 1a is known to affect the mGluR–IP_3 signalling by interfering with long Homers, which bind to mGluRs and IP_3Rs, and by directly activating group I mGluRs (Fagni *et al.*, 2002). This pathway might be responsible for the present Homer 1a-induced enhancement of Ca^{2+} increase. To test this possibility, key molecules constituting this signalling path were blocked one by one (Fig. 2). The following blockers, bath-applied prior to Homer 1a infusion, abolished the enhancement of Ca^{2+} increase (Fig. 2A and B): the noncompetitive group I mGluR antagonist MPEP (0.19 ± 0.01; $n = 6$); the phospholipase C (PLC) blocker U73122 (0.18 ± 0.01; $n = 5$); IP_3R blocker heparin (0.19 ± 0.01; $n = 6$); and the Ca^{2+} store depletor CPA (0.19 ± 0.01; $n = 4$). With none of these blockers was the Ca^{2+} increase significantly different from control (0.18 ± 0.01; $n = 5$). The competitive group I mGluR antagonist AIDA, however, failed to block the Homer 1a effect (0.28 ± 0.01, $n = 6$, $P < 0.001$ against the control; Fig. 2A and B) in agreement with the earlier report that the noncompetitive blocker MPEP, but not AIDA, antagonizes the effect of Homer 1a as an intracellular agonist of mGluRs (Ango *et al.*, 2001).

It was thus revealed that induction of the enhancement of Ca^{2+} rise by Homer 1a depended on the mGluR–IP_3 signalling. This, however, does not necessarily mean that the maintenance of enhancement depends on the same signalling. To check this point, we applied the mGluR antagonist MPEP after the enhancement had been induced: the enhanced calcium rise survived the bath application of MPEP (0.28 ± 0.01 before application vs. 0.28 ± 0.01 after application; $n = 5$). The IP_3R blocker heparin, applied after the induction, also left the enhancement unchanged: 0.28 ± 0.02 before vs. 0.27 ± 0.01 after ($n = 4$). The latter result strongly suggests that the enhanced part of the Ca^{2+} rise is not represented by calcium release from IP_3Rs.

We then examined the origin of the enhanced part of the Ca^{2+} increase by using the calcium store depletor CPA (Fig. 3), following the method described in our previous report (Yamamoto *et al.*, 2000). After the enhancement of spike-induced Ca^{2+} increase had been established by Homer 1a infusion, the store depletor CPA was bath-applied and spike trains were repeated eight times at 1-min intervals (Fig. 3). Even at the eighth train, the peak Ca^{2+} increase did not significantly differ (0.31 ± 0.02, $n = 6$; Fig 3, 8th) from that at the first train (0.33 ± 0.02, Fig 3, 1st). The peak Ca^{2+} increases remained significantly larger (always $P < 0.01$) than the no-Homer, CPA-alone control (Fig. 3; 1st, 0.19 ± 0.01, $n = 5$; 8th, 0.19 ± 0.02). No sign of store depletion was observed in the Homer 1a-dependent enhancement of Ca^{2+} increase, which is represented by the differences between 'Homer 1a + CPA' cases and "no-Homer, CPA-alone" cases. To

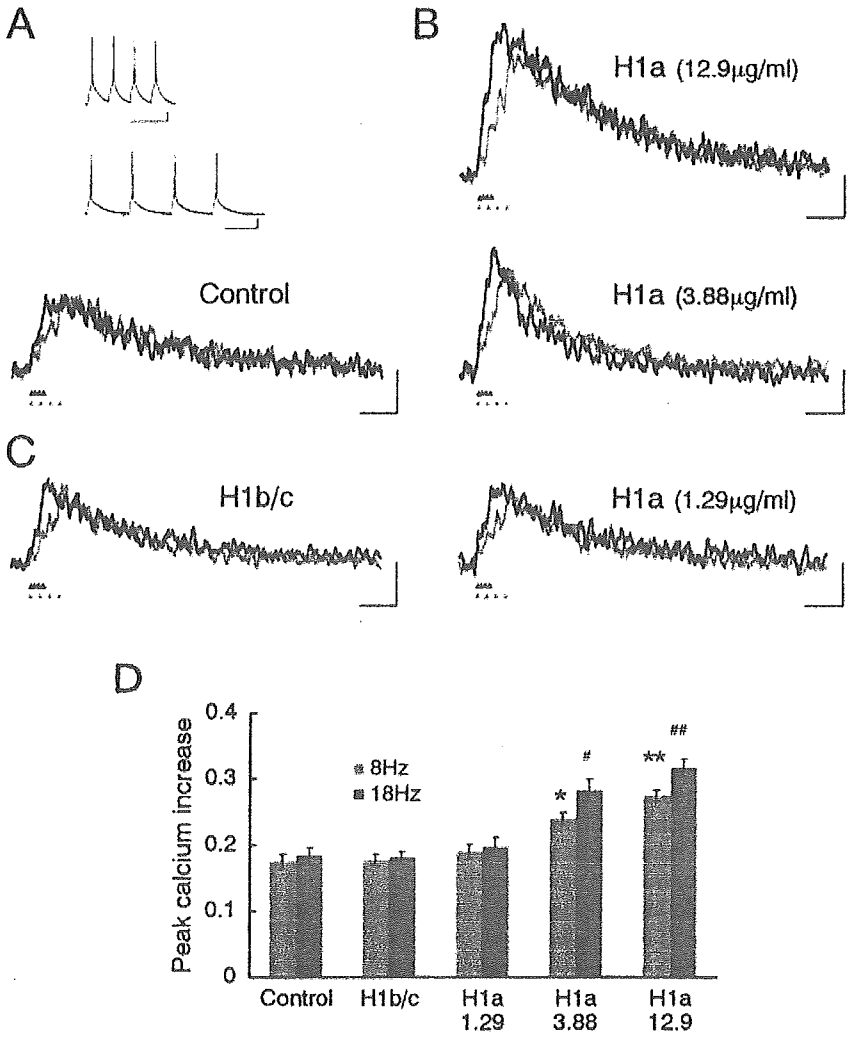

FIG. 1. Intracellular infusion of Homer 1a enhanced spike-induced Ca^{2+} increases in pyramidal cells. (A) Ca^{2+} increases induced by four-spike trains in control cells, to which no Homer was applied (Control; $n = 5$). The frequencies of spike trains were 8 Hz (grey lines) and 18 Hz (black lines). Timings of spike occurrences are shown by grey (8Hz) or black (18 Hz) triangles below the traces. Inset, specimen recordings of spike trains at fixed frequencies (8 Hz, bottom; 18 Hz, top) used for the shown Ca^{2+} measurements from a control neuron (Control). (B) Injection of Homer 1a enhanced spike-induced Ca^{2+} increases in a dose-dependent manner at both frequencies; 12.9 μg/mL ($n = 5$), 3.88 μg/mL ($n = 6$), 1.29 μg/mL ($n = 5$). (C) Injection of Homer 1b/c (3.88 μg/mL; $n = 6$) failed to enhance Ca^{2+} increases at both frequencies. (D) Summary diagram demonstrating average Ca^{2+} increases, separately for cells infused with no Homer, Homer 1b/c or Homer 1a. Only with the lowest concentration used did Homer 1a infusion fail to enhance spike-induced Ca^{2+} increases. $*,^{\#}P < 0.01$, $**,^{\#\#}P < 0.001$. Scale bars, 500 ms and $-0.1\Delta F_{380}/F_{360}$ (A–C), 100 ms and 20 mV (inset in A).

exclude the possibility of an incompetent calcium release, we bath-applied the muscarinic acetylcholine receptor agonist carbachol in combination with Homer 1a (Fig. 3). Carbachol (10 μM) was used because Yamamoto *et al.* (2000) showed that enhancement of spike-induced Ca^{2+} increases under muscarinic acetylcholine receptor activation is maintained by calcium release. When carbachol, Homer 1a and CPA were applied together in triplet (Fig. 3), enhancement of Ca^{2+} increases was initially larger (0.38 ± 0.01, 1st train; $n = 5$, $P < 0.03$) than after application of Homer 1a and CPA in doublet (0.33 ± 0.02, 1st train, filled circles, $n = 6$). This difference, which represents the carbachol-dependent part, was then abolished use-dependently (Fig 3, 2nd and after). Control evidence was thus obtained that calcium stores are still usable with Homer 1a infused. In no-Homer control cells also, carbachol application significantly enhanced Ca^{2+} increases: 0.19 ± 0.01 in no-carbachol control (Figs 3, 1st, $n = 5$) vs. 0.26 ± 0.01 in carbachol cases (1st, $n = 5$, $P < 0.01$). This carbachol-dependent difference, which disappeared use-dependently as in Homer 1a-infused cells, was at a range similar to that observed in Homer-infused cells: 0.33 ± 0.02 vs. 0.38 ± 0.01. These experiments showed that Homer-dependent and carbachol-dependent parts of the enhancement were quite separable and that carbachol-dependent part is attributable to Ca^{2+} release. It is thus likely that the Homer 1a-induced enhancement of Ca^{2+} increase is not maintained by an increase in calcium release but by an increase in calcium influx.

Indeed, the enhanced part turned out to depend on L-type voltage-dependent calcium channels (VDCCs; Fig. 4A and C). In the presence of the L-type VDCC blocker nimodipine, the peak Ca^{2+} increase was 0.14 ± 0.01 ($n = 6$) with Homer 1a infused (Fig. 4A, bottom), which was not significantly different from the no-Homer, nimodipine-alone control (0.13 ± 0.01; $n = 6$; Fig. 4A, top). Thus, nimodipine was shown to abolish the Homer-induced enhancement of Ca^{2+} increase. Furthermore, the L-type VDCC agonist BAY-K 8644, applied alone,

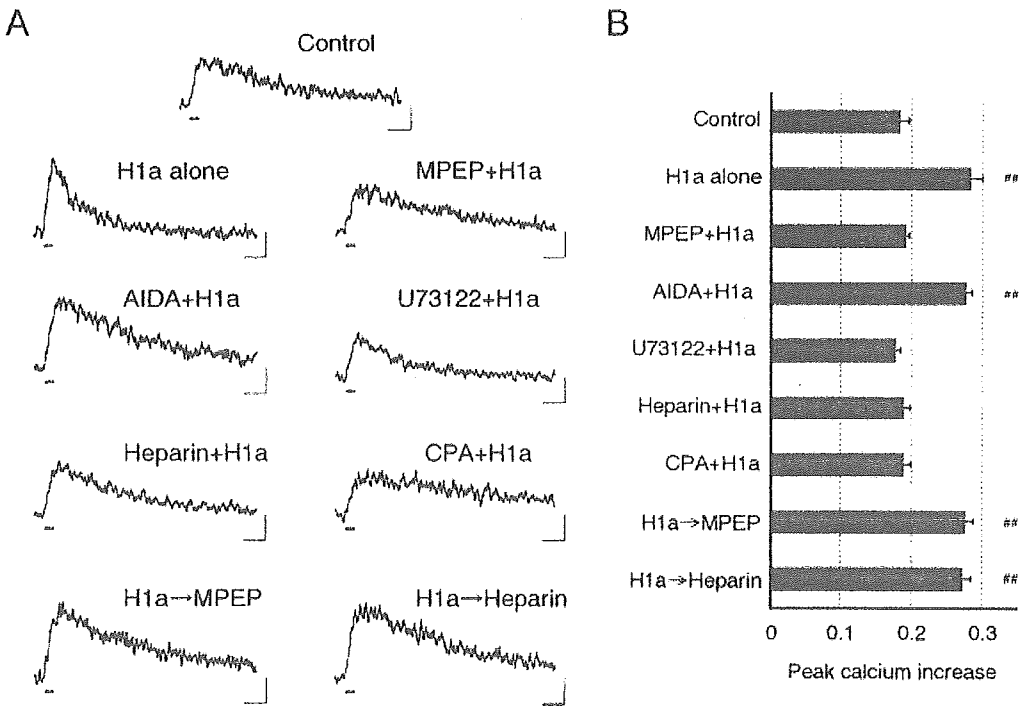

FIG. 2. The Homer 1a-induced enhancement of Ca^{2+} increases depended on the mGluR–IP_3 signalling. (A) Injection of Homer 1a (3.88 μg/mL) enhanced Ca^{2+} increases induced by a four-spike train at 18 Hz (Control vs. H1a). This enhancement was abolished by application of the following drugs prior to Homer 1a infusion: the noncompetitive group I mGluR blocker MPEP, 10 μM (MPEP + H1a; $n = 6$), the PLC inhibitor U73122, 4 μM (U73122 + H1a; $n = 5$), the IP_3R blocker heparin, 4 mg/mL (Heparin + H1a; $n = 6$), or the Ca^{2+} store depletor CPA, 30 μM (CPA + H1a; $n = 4$). Prior application of the competitive group I mGluR antagonist AIDA, 1 mM (AIDA + H1a; $n = 6$) failed to suppress the enhancement, indicating that glutamate-mediated activation of mGluRs is not needed. The enhancement, once induced with Homer 1a alone, survived later application of 10 μM MPEP (H1a → MPEP; $n = 5$) or 4 mg/mL heparin (H1a → Heparin; $n = 4$), indicating that the mGluR–IP_3 signalling is needed for induction but not for maintenance of the Homer 1a-induced enhancement of Ca^{2+} increases. (B) Summary diagram of averaged peak Ca^{2+} increases in the absence or presence of blockers of the mGluR–IP_3 signalling; $^{\#\#}P < 0.001$. Scale bars, 500 ms and $-0.1\Delta F_{380}/F_{360}$ (A).

enhanced spike-induced Ca^{2+} influx, with the peak (0.29 ± 0.01, $n = 5$) becoming significantly greater than the control with no drug (0.18 ± 0.01, $n = 5$, $P < 0.001$; Fig. 4B and C). By contrast, the agonist applied to neurons with Homer 1a infused did not significantly augment the peak amplitude any further (0.29 ± 0.01; $n = 6$), indicating that the agonist effect was occluded by Homer 1a that was applied beforehand (Fig. 4B and C).

Facilitation of L-type VDCC currents in neurons infused with Homer 1a

To confirm the data based on photometry, voltage-activated Ca^{2+} currents were measured. In voltage-clamp experiments, voltage steps from the holding voltage of −70 mV to various depolarized voltages were imposed with (Fig. 5, A2) or without (Fig. 5, A1) Homer 1a infused. With Homer 1a infused, the peak Ca^{2+} current was evoked by the voltage step from −70 mV to −10 mV (Figs 1 and 2, no drugs; 2.12 ± 0.09 nA, $n = 6$, $P < 0.01$), which was significantly larger than the control (1.61 ± 0.05 nA, $n = 5$; Fig. 5, A1, no drugs). Hereafter, when we refer to the peak current it is under these space-clamp conditions.

Pharmacological experiments confirmed that the enhancement of Ca^{2+} currents was maintained by up-regulation of L-type VDCCs (Fig. 5B). Fist of all, currents that we measured were completely suppressed by blocking all classes of VDCCs with a high concentration of Ni^{2+} (500 μM; Fig. 5B): Control, 0.07 ± 0.01 nA, $n = 5$ and Homer 1a, 0.11 ± 0.04 nA, $n = 5$. Then, bath-application of the L-type VDCC blocker nimodipine suppressed Ca^{2+} currents in Homer 1a-infused neurons. The peak current in neurons with Homer 1a infused (1.16 ± 0.13 nA, $n = 5$) was not significantly different from the no-Homer control (1.23 ± 0.11 nA, $n = 5$). It was thus shown that the Homer 1a-induced enhancement of Ca^{2+} currents depends on L-type VDCCs.

On the other hand, neither the P/Q-type VDCC blocker ω-agatoxin, the N-type VDCC blocker ω-conotoxin nor the T-type VDCC blocker Ni^{+} (low concentration; 50 μM) abolished the Homer 1a-induced enhancement of Ca^{2+} currents (Fig. 5B). The Homer-induced enhancement of the currents was still significant with bath application of ω-agatoxin: control, 1.37 ± 0.04 nA, $n = 4$ vs. Homer 1a, 1.79 ± 0.13 nA, $n = 5$; $P < 0.03$. Application of ω-conotoxin left the enhancement significant: control, 1.20 ± 0.04 nA, $n = 4$ vs. Homer 1a, 1.68 ± 0.08 nA, $n = 5$; $P < 0.01$. Also, Ni^{2+} (50 μM) allowed Homer 1a-infused cells to exhibit a significant enhancement (1.84 ± 0.15 nA, $n = 4$, $P < 0.05$) as compared to the no-Homer, Ni^{2+}-alone control (1.43 ± 0.05 nA, $n = 5$).

Involvement of L-type VDCCs was further supported by experiments with the L-type VDCC agonist BayK8644. Bath application of BayK8644 alone significantly enhanced Ca^{2+} currents without Homer 1a (Fig. 5, A1, BayK8644; 2.20 ± 0.14 nA, $n = 4$, $P < 0.02$). Once BayK8644 enhanced Ca^{2+} currents, this occluded the effect of Homer 1a (Fig. 5A, BayK8644, Control vs. H1a). In Homer 1a-infused cells, Ca^{2+} currents measured in the presence of the agonist (2.15 ± 0.10 nA, $n = 5$) were not significantly different from

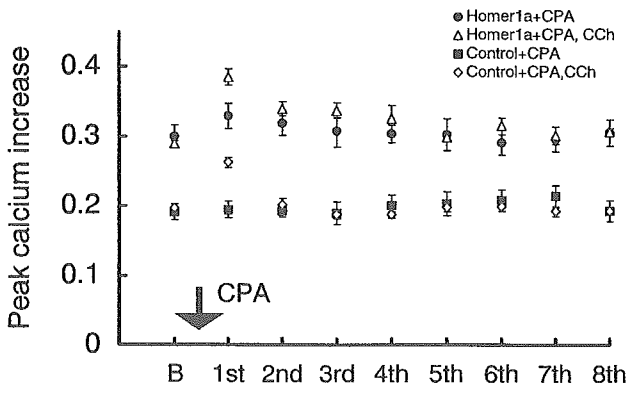

FIG. 3. Maintenance of the Homer 1a-induced enhancement of Ca^{2+} increases under calcium store depletion. The plots show time-courses of the peak Ca^{2+} increases during repetition of spike trains (abscissa; 1st to 8th trains) in various conditions: with Homer 1a and CPA (●, $n = 6$); with Homer 1a, carbachol (CCh, 10 μM) and CPA together (△, 10 and 30 μM, $n = 5$); with no Homer, but CPA (■, 30 μM, $n = 5$); with no Homer, but CPA as well as CCh (◇, $n = 5$). At the timing indicated by the arrow, CPA was bath-applied, with or without CCh; B, before application. Even after eight episodes of spike trains, Ca^{2+} increases for both Homer groups (top two series; △ and ●) stayed higher than the two kinds of no-Homer controls (bottom two series; ◇ and ■). In cells with CCh applied (open symbols), Ca^{2+} releases were initially greater than in the respective no-CCh cases (filled symbols), and then these differences disappeared use-dependently. Calcium release appears to substantiate this CCh-dependent part of the enhancement, but not the Homer 1a-dependent part. Thus, the Homer 1a-induced enhancement is maintained most probably in the form of increased Ca^{2+} influx. The concentration of Ca^{2+} in the bathing medium was 2.5 mM here, but was 3.75 mM in Yamamoto *et al.* (2000).

those measured without BayK8644 bath-applied (2.12 ± 0.09 nA, $n = 6$; Fig. 5, A2, No drug vs. BayK8644). These findings point to involvement of L-type VDCCs in Homer 1a-induced enhancement of Ca^{2+} increases. A further confirmation may come from another finding that a partial (33%) substitution of Ca^{2+} by barium in the bathing medium occluded the Homer 1a effect (Fig. 5B, Barium): control, 2.20 ± 0.06 nA, $n = 4$ vs. Homer 1a, 2.13 ± 0.07 nA, $n = 4$.

Just as for the Homer 1a-induced enhancement of Ca^{2+} fluorescence, the enhancement of Ca^{2+} currents was likely to depend on the mGluR–IP_3 signalling (Fig. 6). Induction of the enhancement was abolished by the mGluR antagonist MPEP, as was evident from the comparison between the currents in neurons with Homer 1a infused (1.67 ± 0.06 nA, $n = 5$) and in those without Homer 1a infused (1.60 ± 0.03 nA, $n = 5$; Fig. 6, A2). The IP_3R blocker heparin also abolished the Homer 1a effects; the current measured with Homer 1a was reduced to 1.67 ± 0.04 nA ($n = 6$), which was not significantly different from those measured without Homer 1a (1.60 ± 0.03 nA, $n = 5$; Fig. 6, A1). Interestingly, IP_3 infusion alone failed to mimic Homer 1a infusion. With IP_3 alone infused, Ca^{2+} currents became 1.67 ± 0.07 nA ($n = 4$), which was not significantly different from the no-IP_3, no-Homer control (Fig. 6B). Activation of the mGluR–IP_3 signalling was thus insufficient to enhance L-type VDCC currents by itself. A second, as yet unknown, factor must therefore be activated necessarily by Homer 1a, the nature of which has yet to be clarified.

Homer 1a facilitated generation of calcium spikes

Ca^{2+} currents are known to increase in a regenerative manner to elicit Ca^{2+} spikes. Homer 1a-induced enhancement of L-type VDCC currents might influence occurrence of Ca^{2+} spikes in our preparation. With or without Homer 1a infused, we attempted to elicit Ca^{2+} spikes by applying varying intensities of depolarizing currents lasting for 50 ms. Intensities of applied currents ranged from 20 to 240 pA, with the minimum step of 20 pA (Fig. 7, A1, Control, bottom current trace).

Irrespective of whether Homer 1a was infused or not, there was a certain threshold above which Ca^{2+} spikes were generated (Fig. 7, A1). The peak amplitude of the voltage change induced by current injection plotted in each cell (Fig. 7, A2, top). Then, to compare the threshold, these peak voltages were averaged across cells for each experimental group (Fig. 7, A2, bottom). The threshold was significantly lower in Homer 1a-infused neurons ($n = 9$) than the no-Homer control ($n = 10$; $P < 0.01$, Mann–Whitney rank-sum test, $T_1 = 135$, $T_2 = 45$; Fig. 7A). With a partial substitution of Ca^{2+} by barium (33%), the threshold became significantly lower, even without Homer 1a infusion, than the no-Homer, no-barium control ($n = 7$; $P < 0.01$, $T_1 = 28$, $T_2 = 91$; Fig. 7, B1, Control; Fig. 7, B2, dotted solid traces). In neurons infused beforehand with Homer 1a, no further lowering of threshold was induced by barium substitution ($n = 7$, $P > 0.05$, T = 49; Fig. 7, B1, H1a; Fig. 7, B2, solid traces), indicating that the effects of Homer 1a infusion and barium substitution were occluded. These results are consistent with the interpretation that the effect of Homer 1a on the threshold for Ca^{2+} spikes is attributable to Homer 1a-induced facilitation of L-type VDCCs, given that barium substitution is known to reduce Ca^{2+}-dependent inactivation characteristic of L-type VDCCs and may therefore enhance currents across these channels (Dolphin, 1996).

Calcium currents were enhanced after ECS

Homer 1a is known to be expressed by seizure activity or LTP-inducing tetanic stimulation (Brakeman *et al.*, 1997; Kato *et al.*, 1997). We showed that Homer 1a induced by ECS hyperpolarizes rat neocortex pyramidal cells, which was disrupted by coapplication of anti-Homer 1a antibody (Sakagami *et al.*, 2004, 2005). We here tested whether ECS-induced Homer 1a, as well as infused Homer 1a, up-regulates L-type VDCC currents. Brief electrical shocks were applied to the heads of rats through two electrodes, placed one on each ear, and then the animals were returned to the cage. Seizure was thereby elicited, lasting for a minute or two, during which the whole body of the animal became spastic, with the eyelids closed and the extremities rigidly flexed. Then, the rats stayed immobile for minutes in a fixed position in the cage, with the eyelids opened and the extremities relaxed. However, 10 min after the electrical shock, the rats looked normal. The animals were killed at 10–20 min (early recording group) or 6 h (late recording group) after the shock, and brains were removed immediately for slice cutting. Ca^{2+} currents were recorded from layer II-III pyramidal cells at 1–5 h plus 10–20 min (early) or 7–11 h plus 10–20 min (late recording) after ECS, and 1–5 h after slice cutting for both groups.

Similarly to experiments done with Homer 1a infusion, voltage steps from the holding voltage of −70 mV to various levels of depolarization were imposed in slices obtained from ECS rats. Peak Ca^{2+} currents in slices from the early group ECS rats were significantly enhanced (2.23 ± 0.10 nA, $n = 5$, $P < 0.01$; Fig. 8A) compared to the no-ECS control (1.61 ± 0.05 nA, $n = 5$; Fig. 5A). An additional application of Homer 1a did not significantly alter Ca^{2+} currents in slices from the early recording group (2.34 ± 0.05 nA, $n = 5$; Fig. 8A), indicating occlusion of ECS effects by Homer 1a. Infusion of anti-Homer 1a antibody significantly reduced Ca^{2+} currents (1.65 ± 0.10 nA, $n = 5$, $P < 0.001$; Fig. 8C) in slices from the early group; this is not significantly different from the no-ECS, no-Homer control (1.61 ± 0.05 nA, $n = 5$; Fig. 5A).

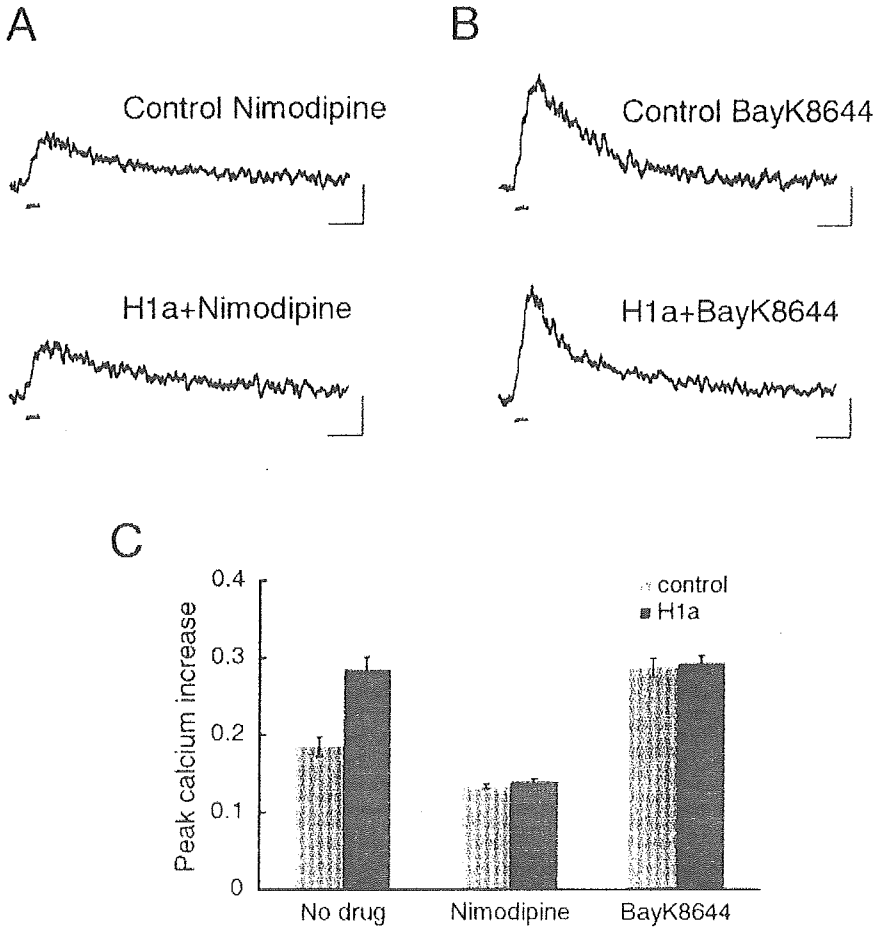

FIG. 4. Dependence of Homer 1a-induced enhancement of Ca^{2+} increases on L-type Ca^{2+} channels. (A) Spike-induced Ca^{2+} increases in the presence of nimodipine (20 μM), an L-type Ca^{2+} channel blocker, without (Control; $n = 6$) or with Homer 1a infused (H1a; $n = 6$). Nimodipine prevented the enhancement. (B) Spike-induced Ca^{2+} increases in the presence of the L-type Ca^{2+} channel agonist BayK8644 (1 μM), without (Control; $n = 5$) or with Homer 1a infused (H1a; $n = 5$). BayK8644 applied alone enhanced the peak Ca^{2+} increase. Homer 1a failed to further enhance Ca^{2+} increase under BayK8644 application. Scale bars, 500 ms and $-0.1\Delta F_{380}/F_{360}$. (C) Summary diagram of averaged peak Ca^{2+} increases in the presence of nimodipine or BayK8644.

In cells from the late ECS group, on the other hand, peak Ca^{2+} currents were no longer significantly enhanced (1.68 ± 0.06 nA, $n = 5$; Fig. 8B), pointing to a time-dependence of the ECS effect. This time-dependence is consistent with an involvement of Homer 1a, which is a transiently inducible immediate–early gene. Homer 1a infusion enlarged Ca^{2+} currents in cells from the late group (2.24 ± 0.07 nA, $n = 5$; Fig. 8B, left vs. right), indicating that cells had been short of, but were still responsive to, Homer 1a. Anti-Homer 1b/c antibody, unlike anti-Homer 1a antibody, failed to show a blocking effect on Ca^{2+} currents (2.21 ± 0.06 nA, $n = 6$; Fig. 8C). It is thus suggested that Homer 1a induced by ECS mediates the enhancing effect of ECS on Ca^{2+} currents.

Discussion

The present experiments revealed (i) that intracellular infusion of Homer 1a protein enhanced spike-induce Ca^{2+} influx, most likely via L-type VDCCs, in rat visual cortex pyramidal cells; (ii) that this enhancement requires mGluR–IP_3 signalling; (iii) that the VDCC enhancement was accompanied by a decrease in the threshold for Ca^{2+} spikes; and (iv) that a similar enhancement of spike-induced Ca^{2+} influx was observed in slices obtained from rats subjected to ECS. This enhancement of Ca^{2+} influx may mediate effects of Homer 1a in synaptic regulation.

Homer 1a as an activity-dependent regulator of neural excitability

Homer 1a, up-regulated by intense neural activity, is known to increase the threshold for inducing amygdala kindling (Potschka *et al.*, 2002) and hippocampus LTP (Schwarz *et al.*, 2003), consistently with the implication for a Homer-mediated negative feedback regulation in neural activity (Brakeman *et al.*, 1997; Kato *et al.*, 1997). It is not self-evident, however, whether this line of understanding on Homer 1a function fits well with the present Homer 1a-mediated up-regulation of L-type VDCCs. Ca^{2+} influx plays a triggering role in many neural processes including transmitter release, short-term and long-term plasticity, path finding, and expression of immediate–early genes (Berridge, 1998). Because of such diverse effects on neural activity, intracellular Ca^{2+} influxes are often regarded as elevating neural excitability, driving further spike firing. However, although spike firing necessarily leads to Ca^{2+} influx, Ca^{2+} influx does not always

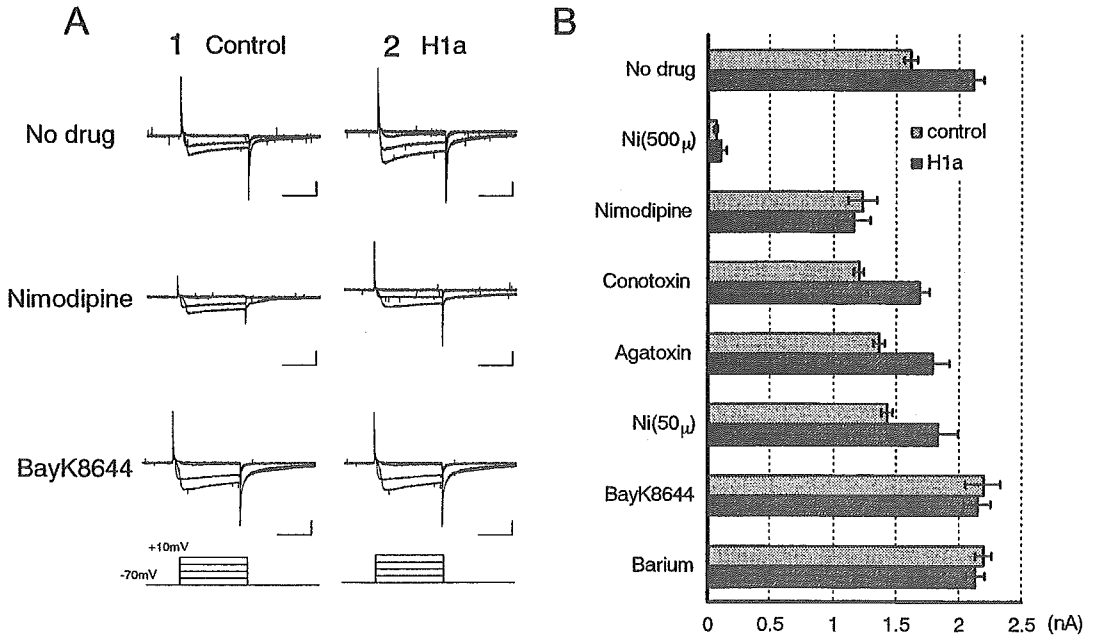

FIG. 5. Enhancement of Ca^{2+} currents by Homer 1a. (A) Effects of bath-applied nimodipine or BayK8644 on Ca^{2+} currents (A2, H1a) with or (A1, Control) without Homer 1a infused. Homer 1a infusion enhanced Ca^{2+} currents (A2, No drug; $n = 6$). Nimodipine (20 μM), bath-applied prior to Homer 1a infusion, abolished the effect of Homer 1a (A2, Nimodipine; $n = 5$). BayK8644 (1 μM) enhanced Ca^{2+} currents without Homer 1a (A1, BayK8644; $n = 5$), and Homer 1a occluded this effect of the agonist (A2, BayK8644; $n = 6$). (B) Ca^{2+} currents evoked under various conditions. The peak intensities of Ca^{2+} currents (evoked by the step to −10 mV) are compared. Homer 1a infusion enhanced the current. A high concentration of Ni^{2+} (500 μM; $n = 5$ with Homer 1a, $n = 5$ without) eliminated the whole current, indicating that what we recorded was indeed Ca^{2+} current. A low concentration of Ni^{2+} (50 μM; $n = 4$ with Homer 1a, $n = 5$ without), ω-conotoxin (1 μM; $n = 5$ with Homer 1a, $n = 4$ without) and ω-agatoxin (100 nM; $n = 5$ with Homer 1a, $n = 4$ without) all failed to abolished the Homer effect, suggesting a specific involvement of L-type Ca^{2+} channels. A partial substitution of extracellular Ca^{2+} ions with barium (Barium; $n = 4$), as well as application of BayK8644 (BayK8644; $n = 5$), enhanced Ca^{2+} currents by itself. Scale bars, 100 ms and 1 nA.

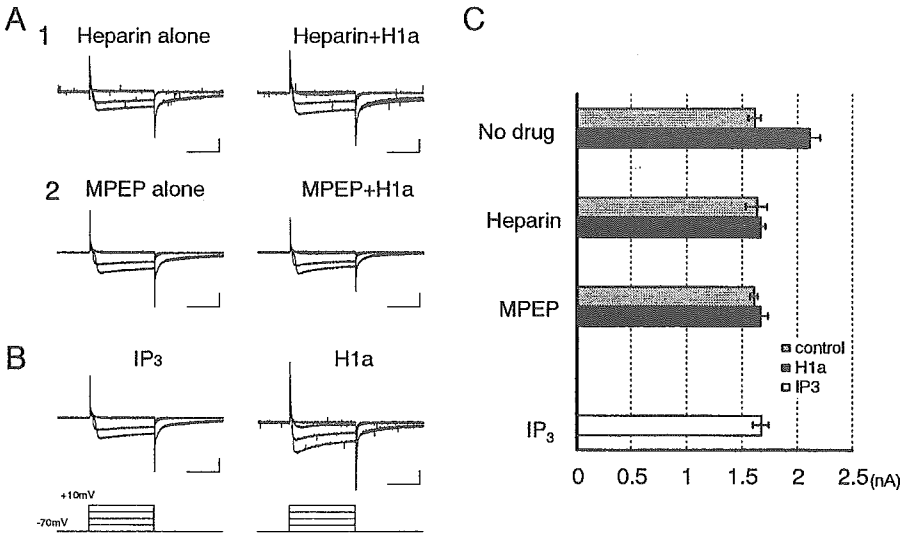

FIG. 6. Induction of Ca^{2+} current enhancement by Homer 1a depends on the mGluR–IP_3 signalling. (A) A prior application of 4 mg/mL heparin (A1; Heparin + H1a, $n = 6$) or 10 μM MPEP (A2; MPEP + H1a, $n = 5$) prevented Homer 1a from enhancing Ca^{2+} currents. Heparin or MPEP alone did not interfere with Ca^{2+} currents (A1 and A2, Heparin alone, MPEP alone; both $n = 5$). (B) Ca^{2+} currents measured with Homer 1a (H1a) or IP_3 alone (IP3) infused intracellularly. Infusion of IP_3 alone (200 μM; $n = 4$) failed to mimic the Homer 1a effect. (C) The peak Ca^{2+} currents (evoked by steps to −10 mV) are compared. Scale bars, 100 ms and 1 nA.

cause an increase in neural excitability. Indeed, as clearly seen in the following cases, neuronal excitability can be reduced by Ca^{2+} influx.

First, spike frequency adaptation is a typical example of negative feedback regulation of spike firing, in which spike-induced Ca^{2+} influx through VDCCs opens SK channels responsible for the medium spike afterhyperpolarization (mAHP) in neocortex and hippocampus neurons (Sah, 1996). Second, our recent report has shown that IP_3R-mediated Ca^{2+} release triggered by Ca^{2+} influx (IP_3-assisted CICR; Yamamoto *et al.*, 2000) is targeted specifically on SK channels, thereby enhancing mAHP supra-linearly in visual cortex pyramidal

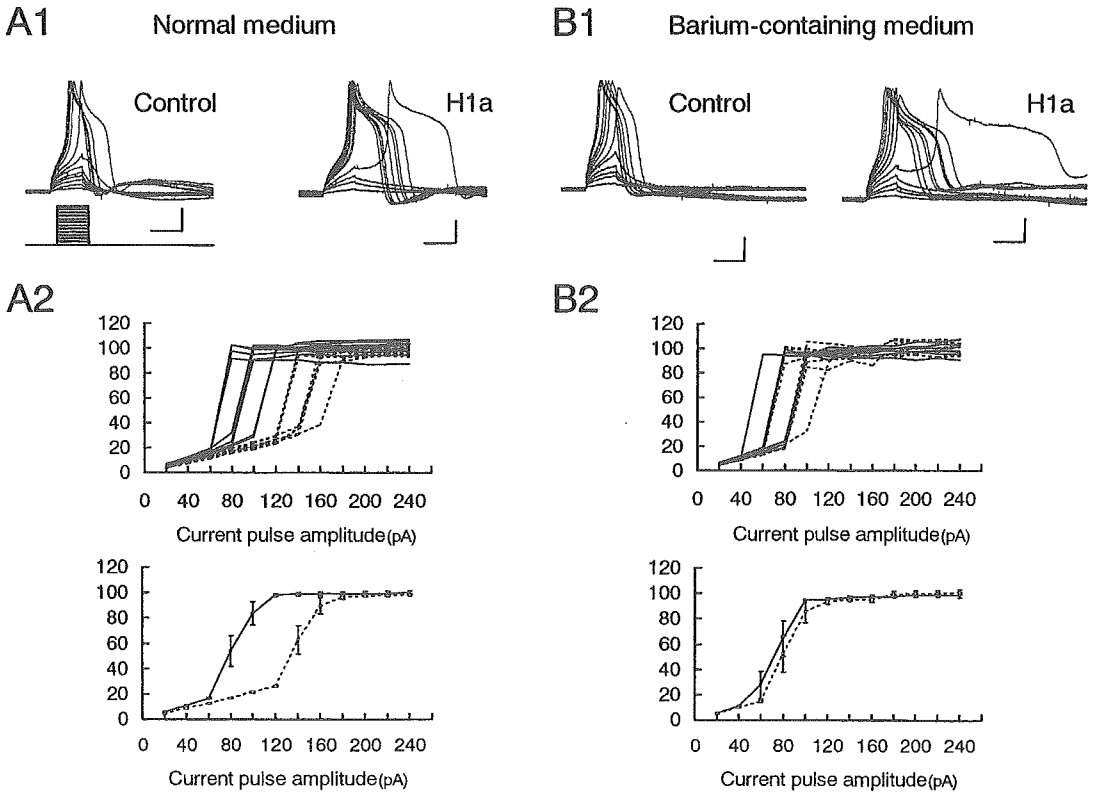

FIG. 7. Homer 1a-induced decrease in the threshold for Ca^{2+} spikes. (A1) Superimposed voltage responses evoked by depolarizing currents of various intensities. Bottom traces represent intensities and time courses of the injected currents and apply to all the recordings shown in A1 and B1. Under Na^{+} channel blockade, large voltage shifts appear in an all-or-none fashion: hence, Ca^{2+} spikes. The threshold current intensity for Ca^{2+} spikes was smaller with Homer 1a infused (H1a; $n = 9$) than in controls (Control; $n = 10$). (A2) The peak amplitude of the voltage shift (in mV) is plotted against the current intensity, individually for each cell (top) and collectively after averaging across cells (bottom). Homer 1a infusion shifted the curves leftward (solid lines) relatively to the curve for the no-Homer control (dotted lines). (B1 and B2) Ca^{2+} spikes were generated in barium-containing bathing medium (Ca^{2+} 1.67 mM and barium 0.83 mM instead of Ca^{2+} 2.5 mM only), and displayed in the same manner as those generated in control medium (A1 and A2). The threshold for Ca^{2+} spikes was already reduced without Homer 1a infusion (B1, Control; $n = 7$). The occlusion of barium and Homer effects was evident (B1, H1a; $n = 7$). Scale bars, 50 ms and 20 mV (A1 and B1).

cells (Yamada *et al.*, 2004). Third, Sun *et al.* (2003) reported that Ca^{2+} influx through L- and N-type VDCCs is specifically coupled with big-conductance calcium-dependent potassium (BK) channels in mouse neocortex pyramidal cells. Fourth, not just Ca^{2+} influx through VDCCs but also those through *N*-methyl-D-aspartate receptors (NMDARs) are reported to relate closely to BK channels in olfactory bulb granule cells, thereby producing a slow extrasynaptic inhibition mediated by glutamate (Isaacson & Murphy, 2001). Moreover, Ca^{2+} release from ryanodine receptors is also known to activate BK channels in cultured bullfrog sympathetic ganglion cells, resulting in attenuation of spike firing (Akita & Kuba, 2000).

Hence, in many neural systems, enhanced Ca^{2+} increases participate in a feedback regulation of spike firing. The present results are therefore consistent with key roles that Homer 1a is suggested to play in negative feedback regulation of neural excitability.

Postulated functional relevance

By virtue of Ca^{2+} spikes that occur to various extents at locations between synaptic sites and the soma, synaptic inputs generated at dendrites and passively propagated to the soma could vary their contribution to spike generation at the soma (Magee & Johnston, 1997; Helmchen *et al.*, 1999; Larkum *et al.*, 1999; Häusser *et al.*, 2000). Ca^{2+} spikes are known thereby to affect synaptic integration at the soma. If Homer 1a made Ca^{2+} spikes easier to evoke, as shown in the present study, synaptic inputs would have greater electrotonic influence on synaptic integration in the soma. Then, a single synaptic potential would contribute more to somatic spike generation. However, our recent experiments have shown that the probability of spike generation is reduced at the soma with Homer 1a infused or expressed (Sakagami *et al.*, 2004, 2005). Taken together, it follows that expression of Homer 1a will augment synaptic potentials and, at the same time, reduce somatic excitability.

The consequences of such a combination of Homer 1a-induced effects are yet to be studied, though several lines of interpretation may be allowed. First, these effects combined together might serve to improve the signal : noise ratio in synaptic integration. Somatic spike firing should be less easy with Homer 1a expressed because of its hyperpolarizing action. Then, noise-level synaptic inputs that do not contribute to Ca^{2+} spike generation would participate in synaptic integration with a much smaller weight than before Homer 1a expression. A second interpretation would be that a reduction in neuronal excitability (Sakagami *et al.*, 2004, 2005) is the principal effect of Homer 1a, and Ca^{2+} spike facilitation may play a secondary, compensatory, role. With somatic hyperpolarization, even a strong synaptic input may fail to induce faithful spike firing at the soma. Facilitation of calcium spikes by Homer 1a might just compensate such bias in disfavour of somatic spike firing. As a third possibility, synaptic plasticity may be affected. The two Homer effects combined together would exaggerate presynaptic strengths and urge

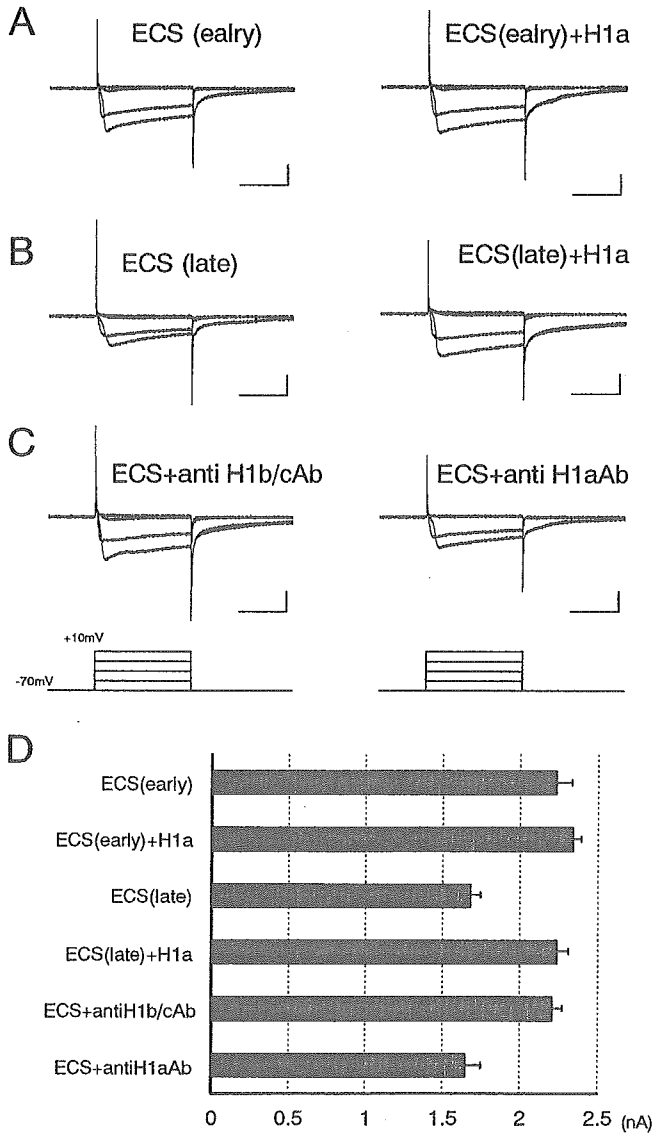

FIG. 8. Enhancement of Ca^{2+} current by ECS and its dependence on Homer 1a. (A and B) Voltage-clamp recordings of Ca^{2+} currents were made at 1–5 h plus 10–20 min after ECS [A; ECS(early)] or 7–11 h after [B; ECS(late)]. Homer 1a was (A and B, right; both $n = 5$) or was not (A and B left; both $n = 5$) infused. Homer 1a infusion enlarged Ca^{2+} currents in cells from the late group (B, left vs. right). (C) Anti-Homer 1a Ab ($n = 5$), but not anti-Homer 1b/c Ab ($n = 6$), abolished the effect of ECS in the early ECS cases. (D) The peak amplitudes of Ca^{2+} current (elicited by steps to −10 mV) were compared. Scale bars, 100 ms and 1 nA (A–C).

underestimation of postsynaptic activities. Such discrepant estimation of pre- and postsynaptic activities may lead to perturbation of synaptic plasticity, as theoretical considerations suggest (Bienenstock *et al.*, 1982; Dayan & Abbott, 2001). Indeed, it has been reported that LTP in the hippocampus is more difficult to induce in transgenic mice that overexpress Homer 1a and, inversely, LTP is enhanced in *Homer 1* knockouts (Schwarz *et al.*, 2003). Also, Homer 1a overexpression is known to elevate the threshold for inducing amygdala kindling, another form of synaptic plasticity (Potschka *et al.*, 2002). Finally, in visual cortical layer II-III cells, the same tissue as used here, activation of group I mGluRs are known to relate to induction of synaptic plasticity (Kato, 1993).

Intracellular signals stimulated by Homer 1a infusion

The present study revealed that the mGluR–IP_3 signalling is required for the Homer 1a-iduced enhancement of L-type VDCCs, by using the blockers of mGluRs and IP_3Rs and the Ca^{2+} store depletor CPA. However, activation of this pathway is not sufficient, because infusion of IP_3 failed to mimic the Homer 1a effect. Clearly, activation of two paths of signalling is needed to achieve the present Homer effect: the mGluR–IP_3 signalling and a second, as yet unknown, signalling.

The requirement of the mGluR–IP_3 signalling seems to be consistent with the role of Homer 1a as an intracellular agonist for mGluRs (Ango *et al.*, 2001). Homer 1a is known to stimulate group I mGluRs without the aid of its authentic ligand glutamate, and can therefore be regarded as an activator of the mGluR–IP_3 signalling (Ango *et al.*, 2001). In the present experiments, the noncompetitive antagonist of group I mGluRs MPEP, but not the competitive blocker AIDA, suppressed the Homer 1a-induced enhancement of Ca^{2+} influx. Interestingly, the same differential effects of the competitive and noncompetitive antagonists have been reported on Homer 1a-mediated activation of group I mGluRs expressed in cerebellar granule cells and HEK cells (Ango *et al.*, 2001). Thus, the present finding supports the view that Homer 1a acts as an activator of the mGluR–IP_3 signalling.

As for the second, as yet unknown, signalling required for the present Homer 1a effect, the results reported in Kammermeier *et al.* (2000) seems to be suggestive. They showed that mGluR-mediated modulation of N-type VDCCs in superior cervical ganglion neurons is decreased by artificial expression of Homer 1b/c, which is prevented by coexpression of Homer 1a. Their interpretation is that long Homers tighten the coupling between mGluRs and IP_3Rs by their self-dimerizing coiled-coil domains, with the bias towards relative disfavour of the coupling between mGluRs and VDCCs, and Homer 1a acts as the dominant negative regulator. Thus, molecular linkage with Homer 1b/c and disruption thereof by Homer 1a may determine the ranking of relative strengths among various possible couplings made up of several classes of receptors or channels. The relative influence of the mGluR–IP_3 signalling on L-type VDCCs may likewise be determined by the interaction of long and short Homers. Then, Homer 1a infusion in the present experiments might optimise the distance or strength between L-type VDCCs and the mGluR–IP_3 pathway and, without such optimisation, activation of the mGluR–IP_3 pathway might never be able to up-regulate L-type VDCCs. This sort of optimisation, mediated by physical molecular coupling rather than diffusible factors, may be the second necessary condition required in the present experiments. On the other hand, a direct physical coupling between mGluRs type-1 and P/Q-type VDCCs has been shown and suggested as mediating mGluR-dependent regulation of Ca^{2+} influx (Kitano *et al.*, 2003). Whether this regulation is completely independent of scaffold proteins such as Homers has yet to be examined.

Abbreviations

AIDA, (RS)-1-aminoindan-1,5-dicarboxylic acid; BK channel, big-conductance calcium-dependent potassium channel; CICR, calcium-induced calcium release; CPA, cyclopiazonic acid; ECS, electroconvulsive shock; IP_3, inositol-1,4,5-trisphosphate; IP_3Rs, inositol-1,4,5-trisphosphate receptors; LTP, long-term potentiation; mAHP, medium spike afterhyperpolarization; mGluRs, metabotropic glutamate receptors; MPEP, 2-methyl-6-(phenylethynyl)-pyridine; NMDARs, *N*-methyl-D-aspartate receptors; PCR, polymerase chain reaction; PLC, phospholipase C; SK channel, small-conductance calcium-dependent potassium channel; TEA, tetraethylammonium chloride; TTX, tetrodotoxin; VDCC, voltage-dependent calcium channel.

References

Akita, T. & Kuba, K. (2000) Functional triads consisting of ryanodine receptors, Ca (2+) channels, and Ca (2+)-activated K (+) channels in bullfrog sympathetic neurons. Plastic modulation of action potential. *J. Gen. Physiol.*, **116**, 697–720.

Ango, F., Prezeau, L., Muller, T., Tu, J.C., Xiao, B., Worley, P.F., Pin, J.P., Bockaert, J. & Fagni, L. (2001) Agonist-independent activation of metabotropic glutamate receptors by the intracellular protein Homer. *Nature*, **411**, 962–965.

Berridge, M.J. (1998) Neuronal calcium signaling. *Neuron*, **21**, 13–26.

Bienenstock, E.L., Cooper, L.N. & Munro, P.W. (1982) Theory for the development of neuron selectivity: orientation specificity and binocular interaction in visual cortex. *J. Neurosci.*, **2**, 32–48.

Brakeman, P.R., Lanahan, A.A., O'Brien, R., Roche, K., Barnes, C.A., Huganir, R.L. & Worley, P.F. (1997) Homer: a protein that selectively binds metabotropic glutamate receptors. *Nature*, **386**, 284–288.

Dayan, P. & Abbott, L.F. (2001) *Theoretical Neuroscience: Computational and Mathematical Modeling of Neural Systems*. The MIT Press, Cambridge, USA, pp. 281–293.

Dolphin, A.C. (1996) Facilitation of Ca^{2+} current in excitable cells. *Trends Neurosci.*, **19**, 35–43.

Ehlers, M.D. (2002) Molecular morphogens for dendritic spines. *Trends Neurosci.*, **25**, 64–67.

Fagni, L., Worley, P.F. & Ango, F. (2002) Homer as both a scaffold and transduction molecule. *Sci. STKE*, **137**, RE8.

Feng, W., Tu, J., Yang, T., Vernon, P.S., Allen, P.D., Worley, P.F. & Pessah, I.N. (2002) Homer regulates gain of ryanodine receptor type 1 channel complex. *J. Biol. Chem.*, **277**, 44722–44730.

Häusser, M., Spruston, N. & Stuart, G.J. (2000) Diversity and dynamics of dendritic signaling. *Science*, **290**, 739–744.

Helmchen, F., Svoboda, K., Denk, W. & Tank, D.W. (1999) In vivo dendritic calcium dynamics in deep-layer cortical pyramidal neurons. *Nat. Neurosci.*, **2**, 989–996.

Isaacson, J.S. & Murphy, G.J. (2001) Glutamate-mediated extrasynaptic inhibition: direct coupling of NMDA receptors to Ca (2+)-activated K+ channels. *Neuron*, **31**, 1027–1034.

Isomura, Y. & Kato, N. (1999) Action potential-induced dendritic calcium dynamics correlated with synaptic plasticity in developing hippocampal pyramidal cells. *J. Neurophysiol.*, **82**, 1993–1999.

Kammermeier, P.J., Xiao, B., Tu, J.C., Worley, P.F. & Ikeda, S.R. (2000) Homer proteins regulate coupling of group I metabotropic glutamate receptors to N-type calcium and M-type potassium channels. *J. Neurosci.*, **20**, 7238–7245.

Kato, N. (1993) Dependence of long-term depression on postsynaptic metabotropic glutamate receptors in the visual cortex. *Proc. Natl Acad. Sci. USA*, **90**, 3650–3654.

Kato, A., Fukuda, T., Fukazawa, Y., Isojima, Y., Fujitani, K., Inokuchi, K. & Sugiyama, H. (2001) Phorbol esters promote postsynaptic accumulation of Vesl-1S/Homer-1a protein. *Eur. J. Neurosci.*, **13**, 1291–1302.

Kato, A., Ozawa, F., Saitoh, Y., Hirai, K. & Inokuchi, K. (1997) vesl, a gene encoding VASP/Ena family related protein, is upregulated during seizure, long-term potentiation and synaptogenesis. *FEBS Lett.*, **412**, 183–189.

Kennedy, M.B. (2000) Signal-processing machines at the postsynaptic density. *Science*, **290**, 750–754.

Kitano, J., Nishida, M., Itsukaichi, Y., Minami, I., Ogawa, M., Hirano, T., Mori, Y. & Nakanishi, S. (2003) Direct interaction and functional coupling between metabotropic glutamate receptor subtype 1 and voltage-sensitive Cav2.1 Ca2+ channel. *J. Biol. Chem.*, **278**, 25101–25108.

Larkum, M.E., Zhu, J.J. & Sakmann, B. (1999) A new cellular mechanism for coupling inputs arriving at different cortical layers. *Nature*, **398**, 338–341.

Magee, J.C. & Johnston, D. (1997) A synaptically controlled, associative signal for Hebbian plasticity in hippocampal neurons. *Science*, **275**, 209–213.

Nakamura, T., Barbara, J.G., Nakamura, K. & Ross, W.N. (1999) Synergistic release of Ca^{2+} from IP_3-sensitive stores evoked by synaptic activation of mGluRs paired with backpropagating action potentials. *Neuron*, **24**, 727–737.

Potschka, H., Krupp, E., Ebert, U., Gumbel, C., Leichtlein, C., Lorch, B., Pickert, A., Kramps, S., Young, K., Grune, U., Keller, A., Welschof, M., Vogt, G., Xiao, B., Worley, P.F., Loscher, W. & Hiemisch, H. (2002) Kindling-induced overexpression of Homer 1A and its functional implications for epileptogenesis. *Eur. J. Neurosci.*, **16**, 2157–2165.

Power, J.M. & Sah, P. (2002) Nuclear calcium signaling evoked by cholinergic stimulation in hippocampal CA1 pyramidal neurons. *J. Neurosci.*, **22**, 3454–3462.

Sah, P. (1996) Ca^{2+}-activated K^+ currents in neurons: types, physiological roles and modulation. *Trends Neurosci.*, **19**, 150–154.

Sakagami, Y., Yamamoto, K., Sugiura, S., Inokuchi, K., Hayashi, T. & Kato, N. (2004) Reduction of pyramidal cell excitability by Homer-1a/Vesl-1S injection or by electroconvulsive shock (ECS) that is presumed to induce Homer-1a/Vesl-1S. *Soc. Neurosci. Abstr.*, **516**, 4.

Sakagami, Y., Yamamoto, K., Sugiura, S., Inokuchi, K., Hayashi, T. & Kato, N. (2005) Roles of Homer-1a in homeostatic regulation of pyramidal cell excitability: a possible link to clinical benefits of electroconvulsive shock. *Eur. J. Neurosci.*, **21**, 3229–3239.

Schwarz, M.K., Rozov, A., Hvalby, O., Jensen, V., Worley, P.F. & Seeburg, P.H. (2003) Homer 1 gene products differentially affect long-term changes in synaptic efficiency. *Soc. Neurosci. Abstr.*, **375**, 14.

Sheng, M. & Kim, E. (2000) The Shank family of scaffold proteins. *J. Cell. Sci.*, **113**, 1851–1856.

Sun, X., Gu, X.Q. & Haddad, G.G. (2003) Calcium influx via L- and N-type calcium channels activates a transient large-conductance Ca^{2+}-activated K^+ current in mouse neocortical pyramidal neurons. *J. Neurosci.*, **23**, 3639–3648.

Tu, J.C., Xiao, B., Yuan, J.P., Lanahan, A.A., Leoffert, K., Li, M., Linden, D.J. & Worley, P.F. (1998) Homer binds a novel proline-rich motif and links group 1 metabotropic glutamate receptors with IP_3 receptors. *Neuron*, **21**, 717–726.

Westhoff, J.H., Hwang, S.Y., Scott Duncan, R., Ozawa, F., Volpe, P., Inokuchi, K. & Koulen, P. (2003) Vesl/Homer proteins regulate ryanodine receptor type 2 function and intracellular calcium signaling. *Cell Calcium*, **34**, 261–269.

Yamada, S., Takechi, H., Kanchiku, I., Kita, T. & Kato, N. (2004) Small-conductance Ca^{2+}-dependent K^+ channels are the target of spike-induced Ca^{2+} release in a feedback regulation of pyramidal cell excitability. *J. Neurophysiol.*, **91**, 2322–2329.

Yamamoto, K., Hashimoto, K., Isomura, Y., Shimohama, S. & Kato, N. (2000) An IP_3-assisted form of Ca^{2+}-induced Ca^{2+} release in neocortical neurons. *Neuroreport*, **11**, 535–539.

Yamamoto, K., Hashimoto, K., Nakano, M., Shimohama, S. & Kato, N. (2002a) A distinct form of calcium release down-regulates membrane excitability in neocortical pyramidal cells. *Neuroscience*, **109**, 665–676.

Yamamoto, K., Nakano, M., Hashimoto, K., Shimohama, S. & Kato, N. (2002b) Emergence of a functional coupling between inositol-1,4,5-trisphosphate receptors and calcium channels in developing neocortical neurons. *Neuroscience*, **109**, 677–685.

Young, C.E. & Yang, C.R. (2004) Dopamine D1/D5 receptor modulates state-dependent switching of soma–dendritic Ca^{2+} potentials via differential potein kinase A and C activation in rat prefrontal cortical neurons. *J. Neurosci.*, **24**, 8–23.

Yuan, J.P., Kiselyov, K., Shin, D.M., Chen, J., Shcheynikov, N., Kang, S.H., Dehoff, M.H., Schwarz, M.K., Seeburg, P.H., Muallem, S. & Worley, P.F. (2003) Homer binds TRPC family channels and is required for gating of TRPC1 by IP_3 receptors. *Cell*, **114**, 777–789.

Pax6 is required for production and maintenance of progenitor cells in postnatal hippocampal neurogenesis

Motoko Maekawa[1,3], Noriko Takashima[1,2], Yoko Arai[1], Tadashi Nomura[1], Kaoru Inokuchi[2], Shigeki Yuasa[3] and Noriko Osumi[1,4,*]

[1]*Division of Developmental Neuroscience, Center for Translational and Advanced Animal Research (CTAAR), Tohoku University School of Medicine, 2-1 Seiryo-machi, Aoba-ku, Sendai 980-8575, Japan*

[2]*Mitsubishi Kagaku Institute of Life Sciences (MITILS), Minamiooya 11, Machida, Tokyo 194-8511, Japan*

[3]*Department of Ultrastructural Research, National Institute of Neuroscience, National Center of Neurology and Psychiatry, 4-1-1 Ogawahigashi-machi, Kodaira, Tokyo 187-8502, Japan*

[4]*CREST, Japan Science and Technology Corporation (JST), 4-1-8 Honmachi, Kawaguchi, 332-0012, Japan*

Neurogenesis is crucial for brain formation and continues to take place in certain regions of the postnatal brain including the subgranular zone (SGZ) of the hippocampal dentate gyrus (DG). Pax6 transcription factor is a key player for patterning the brain and promoting embryonic neurogenesis, and is also expressed in the SGZ. In the DG of wild-type rats, more than 90% of total BrdU-incorporated cells expressed Pax6 at 30 min time point after BrdU injection. Moreover, approximately 60% of Pax6$^+$ cells in the SGZ exhibited as GFAP$^+$ cells with a radial glial phenotype and about 30% of Pax6$^+$ cells exhibited as PSA-NCAM$^+$ cells in clusters. From BrdU labeling for 3 days, we found that cell proliferation was 30% decreased at postnatal stages in *Pax6*-deficient *rSey^2*/+ rat. BrdU pulse/chase experiments combined with marker staining revealed that PSA-NCAM$^+$ late progenitor cells increased at the expense of GFAP$^+$ early progenitors in *rSey^2*/+ rat. Furthermore, expression of Wnt ligands in the SGZ was markedly reduced in *rSey^2*/+ rat. Taken all together, an appropriate dosage of Pax6 is essential for production and maintenance of the GFAP$^+$ early progenitor cells in the postnatal hippocampal neurogenesis.

Introduction

Neurogenesis depends on a specific population of cells termed 'neural stem/progenitor cells' (we call here 'neural progenitor cells'). In the mammalian embryonic brain, neural progenitor cells take a feature of 'neuroepithelial cells' or 'matrix cells' (reviewed in Fujita 2003) while the adult brain contains islands of neural progenitor cells in the subventricular zone (SVZ) of the lateral ventricle and in the subgranular zone (SGZ) of the hippocampal dentate gyrus (DG) (Altman & Das 1965 and see reviews by Gage 2000; Alvarez-Buylla *et al.* 2002). These cells possess pluripotent differentiation potential; they can become neurons, astrocytes, or oligodendrocytes.

In hippocampal neurogenesis, dividing precursor cells give rise to daughter cells, which migrate away from the SGZ and start to differentiate into neurons (Seki & Arai 1993; Kuhn *et al.* 1996; Kempermann *et al.* 2003). Several lines of evidence have suggested that there are distinct subtypes of neural progenitor cells in the SGZ. In electron microscopy analysis, there are two types of mitotically active SGZ cells; type B cells that have ultrastructural features of astrocytes with light cytoplasm containing GFAP and multiple processes, rapidly convert into type D cells that are small electron-dense cells and GFAP negative (Seri *et al.* 2001). Another paper (Fukuda *et al.* 2003) has shown two distinct progenitor cells based on morphology, molecular expression, and electrical features: GFAP$^+$ type I cells with lower input resistance (IR) and PSA-NCAM$^+$ type II cells with higher IR. Roughly speaking, type I cells correspond to B cells, while type II cells to D cells. In this paper, we use GFAP$^+$ early progenitors and PSA-NCAM$^+$ late progenitors as clearer definition.

Although adult and embryonic neurogenesis differs in some aspects, there indeed is similarity. In the adult

Communicated by: Tetsuya Taga

**Correspondence*: E-mail: osumi@mail.tains.tohoku.ac.jp

DOI: 10.1111/j.1365-2443.2005.00893.x

hippocampus, GFAP$^+$ early progenitors have the appearance of radial glial cells, and not only do they produce neurons but also provide scaffolding for migration of newly born neurons (Forster *et al.* 2002). These features are quite similar to embryonic radial glial cells that constitute the ventricular zone (Gotz 2003; Tramontin *et al.* 2003). The finding that radial glia-like cells in the adult brain have stem cell properties (Doetsch *et al.* 1997, 1999; Seri *et al.* 2001) leads us to search for intrinsic molecular mechanisms that commonly govern pre- and postnatal neurogenesis.

A transcription factor Pax6 is strongly expressed during brain development in the discrete regions such as the dorsal telencephalon and the ventral hindbrain and serves as one of the key factor for patterning the central nervous system (see reviews by Osumi 2001; Simpson & Price 2002). Specific Pax6 expression is observed in the nucleus of the ventricular zone cells, which are most likely radial glial cells (Gotz 2003). In a spontaneous mutant *Small eye* (*Sey*) mouse that lacks functional Pax6, radial glial cells are less in number and show a distorted morphology, altered gene expression patterns and abnormal cell cycle characteristics (Stoykova *et al.* 1997; Gotz *et al.* 1998; Estivill-Torrus *et al.* 2002). A similar observation that less PCNA-positive cells constitute the thinner ventricular zone in *Small eye* rat mutant (*rSey*^{2}) has also been reported (Fukuda *et al.* 2000). Curiously enough, Pax6 is expressed not only in the embryonic neuroepithelium but also in the adult brain including the SGZ and the SVZ (Stoykova & Gruss 1994; Nakatomi *et al.* 2002; Hack *et al.* 2004, 2005); the above-mentioned regions which are known as the places that neurogenesis persists in adulthood. All these lines of evidences have prompted us to examine the role of Pax6 in postnatal neurogenesis.

Here, we show that Pax6-expressing cells in the SGZ of the hippocampus have a neural progenitor-like character at the molecular and the cellular levels. Detailed BrdU pulse/chase experiments have revealed that the ratio of GFAP$^+$ early progenitor cells in total BrdU$^+$ cells decreased, and instead, PSA-NCAM$^+$ late progenitors increased in the *Pax6*-deficient *rSey*^{2}/+ rat. Therefore Pax6 is necessary for the maintenance of the GFAP$^+$ early progenitor cells in the SGZ. We further searched for Pax6 downstream molecules that are relevant for the proliferation of neural progenitor cells in postnatal hippocampus, and found that expressions of Wnt ligands *Wnt7a* and *Wnt7b* and downstream effecter *Dvl1* are changed in the DG of the *rSey*^{2}/+. Our results suggest that a genetic cascade of Pax6–Wnt is critical for postnatal hippocampal neurogenesis especially at the early step.

Results

Pax6-positive cells express early progenitor markers

Previous studies have reported that Pax6 is expressed in discrete regions of the postnatal brain such as the cerebellum and the limbic system including the olfactory bulb, olfactory cortex, and hippocampus (Stoykova & Gruss 1994; Nakatomi *et al.* 2002; Hack *et al.* 2004). In the present study, we focused on Pax6 expression in the DG of which knowledge on adult neurogenesis has been gathered.

In the DG of the wild-type rat at 4 weeks when the architecture of the hippocampus is established, many Pax6$^+$ cells were observed in unique distribution patterns (Fig. 1A). A majority of Pax6$^+$ cells were located in the SGZ, sometimes in clusters of five to eight cells (Fig. 1A,C). A much smaller number of Pax6$^+$ cells were detectable in the hilus and molecular layer, whereas Pax6$^+$ cells were scarcely found in the granule cell layer (GCL). To elucidate the character of Pax6$^+$ cells, we performed double labeling with various markers for neural progenitor cells, neurons, and astrocytes (Fig. 1B,C). Many of Pax6$^+$ cells co-expressed GFAP, a marker for astrocytes or early progenitors marker (59.0%, 85/144 cells; Fig. 1B,C), and a majority of Pax6/GFAP double-positive cells had processes oriented radially into the GCL of the DG (Fig. 1C,C′; also see Fig. 5E). Pax6$^+$ cells also expressed neural stem cell markers nestin (34.4%, 20/58 cells) and Musashi1 (68.7%, 22/32 cells) (Fig. 1B). About a third of Pax6$^+$ cells co-expressed a late progenitor marker PSA-NCAM (31.5%, 41/130 cells) (Fig. 1B). Contrastingly, Pax6$^+$ cells scarcely expressed neuronal marker NeuN (1.9%: 12/652 cells) (Fig. 1B). These results suggest that Pax6$^+$ cells exhibited the neural progenitor cell-like character.

In immuno-electron microscopy, most of Pax6$^+$ cells had irregular contours and light cytoplasm containing a few ribosomes and glial filaments (Fig. 1D,D′), showing a character of B cell (Seri *et al.* 2001). A few Pax6$^+$ cells had smooth contours and dark scant cytoplasm negative for intermediate filaments (Fig. 1E,E′), showing a character of D cell (Seri *et al.* 2001). We sometimes observed Pax6$^+$ cells that had thinner and feeble glial filaments and scant dark cytoplasm, representing an intermediate character of B cell and D cell. These data suggest that more than half of Pax6$^+$ cells show morphologic features of the GFAP$^+$ early progenitor cells in the DG.

Defects in the DG of *rSey*^{2}/+ rats

In order to elucidate the role of Pax6 in hippocampal neurogenesis, we first observed the DG of *Pax6*-deficient

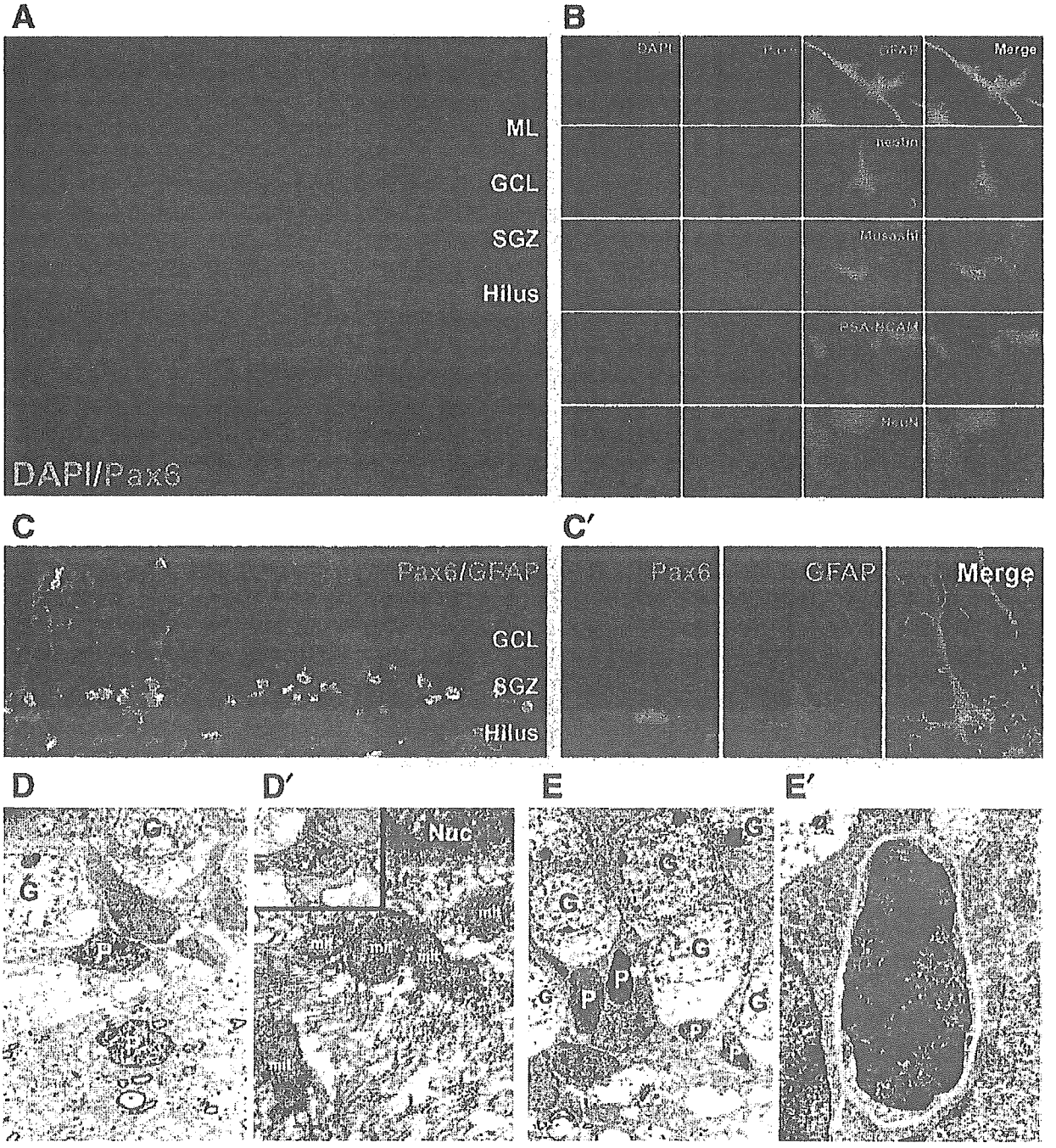

Figure 1 Pax6$^+$ cells in the DG of the 4-week-old wild-type rat. (A) Many Pax6$^+$ cells (magenta) are observed in the subgranular zone (SGZ) and hilus. DAPI, nuclear staining; ML, molecular layer; GL, granular layer. (B) Pax6$^+$ cells co-express an early progenitor marker GFAP, neural stem cell markers nestin and Musashi1, and a late progenitor marker PSA-NCAM, but scarcely co-express a neuronal marker NeuN. Upper, GCL; under, Hilus. (C, C′) Morphological properties of Pax6$^+$ cells. (C) Many of Pax6$^+$ cells show radial glial shape and are often found in clusters in the SGZ. (C′) Pax6$^+$ cell has a GFAP$^+$ radial process. (D, D′, E, E′) Immuno-electron microscopy of Pax6$^+$ cells in the SGZ. P, Pax6$^+$ cells; G, granule cells; U, unknown cells. (D, E) Low magnification (× 1500) of Pax6$^+$ cells in the SGZ. (D′) High magnification (× 10 000) of Pax6$^+$ cell (magenta asterisk in D). Pax6$^+$ cell has irregular contours (magenta line, inset) and light cytoplasm containing a few ribosomes (r) and glial filaments (magenta arrows). Nuc, nucleus; mit, mitochondria. (E′) High magnification (× 5000) of Pax6$^+$ cell (yellow asterisk in E). Pax6$^+$ cells have smooth contours and dark scant cytoplasm negative for intermediate filaments.

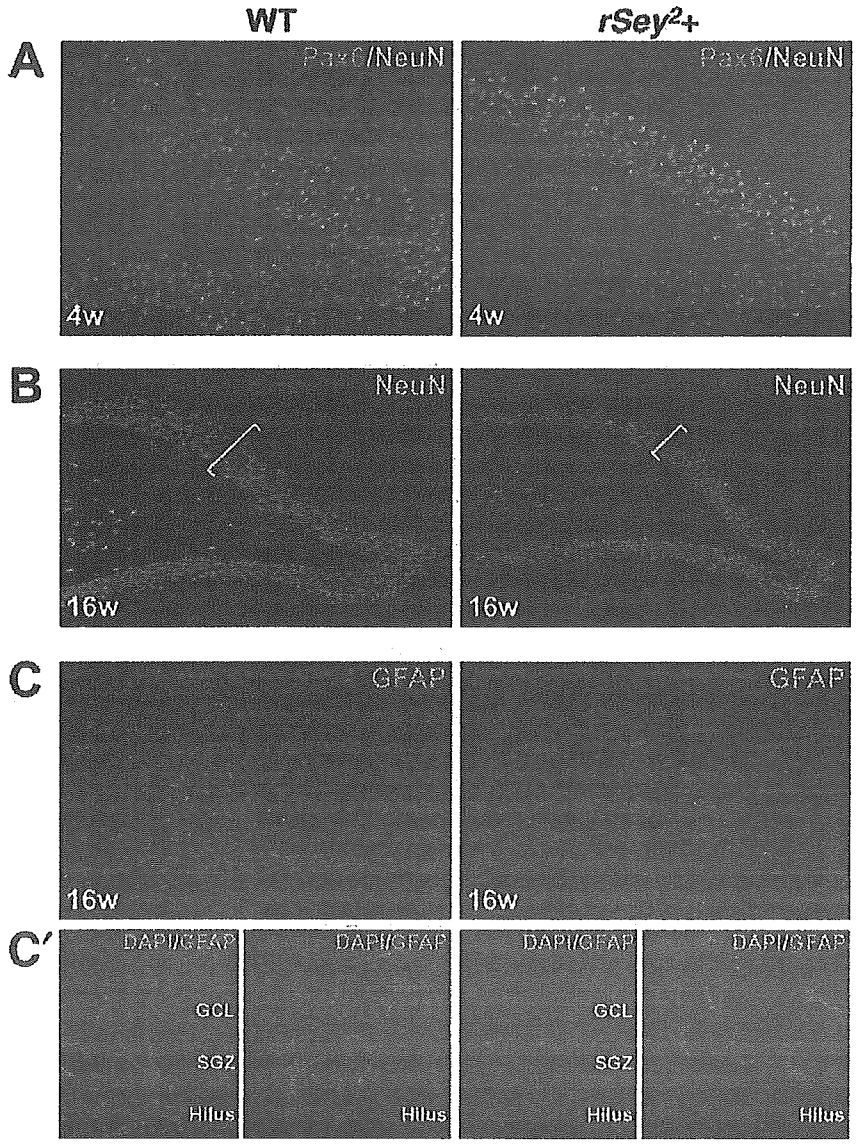

Figure 2 Morphologic defects in DG of *rSey²*/+ rats. (A) In *rSey²*/+ rats at 4 weeks, Pax6-expressing cells are less in number and the expression level of Pax6 is remarkably decreased. (B) In *rSey²*/+ rats at 16 weeks, the thickness (bracket) of the granule cell layer (GCL) in the DG is thinner than that of WT. Granule cells are more packed in the GCL of *rSey²*/+ rats compared with the WT. (C) The number of GFAP$^+$ cells is less in the DG of *rSey²*/+ rats compared to WT. (C′) Radial glial fibers seem shorter and thinner in the DG of *rSey²*/+.

rat (*rSey²*). *rSey²* is a spontaneous mutant that has a nonsense mutation in the *Pax6* gene (Osumi *et al.* 1997), although truncated Pax6 protein is undetectable in the homozygote (our unpublished observation). Since homozygous *Pax6* mutant rats die at birth, heterozygotes (*rSey²*/+) were examined in this study. In the DG of *rSey²*/+ at 4 weeks, we found that the number of Pax6$^+$ cells reduced and that an expression level of Pax6 also decreased (Fig. 2A). We could not observe an apparent difference in the architecture of the DG in *rSey²*/+ rats at this stage.

At 16-week stage, we observed a prominent morphologic defect of the DG *rSey²*/+ rats: the GCL was much thinner and the density of granule cells was higher in the DG of *rSey²*/+ rats compared with the wild type (see brackets in Fig. 2B). We also noticed that the number of GFAP$^+$ cells was decreased and that the processes of GFAP$^+$ radial glial cells were thinner and underdeveloped in the DG of *rSey²*/+ rats (Fig. 2C,C′). This may explain in part why granule cells were more packed in the DG of *rSey²*/+ rats; there may be less spaces among granule cells because of thinner and underdeveloped radial glial processes. The previously mentioned character of Pax6-expressing cells in the DG of the wild type and the abnormalities in the DG of *rSey²*/+ rats raised a possibility that the total number of new neurons in postnatal hippocampus is decreased in the haplo-insufficient condition of the *Pax6* gene.